Ca II H_{2V} AND K_{2V} CELL GRAINS

(Invited Review)

ROBERT, J. RUTTEN[1] and HAN UITENBROEK[1, 2]

(Received 28 January, 1991)

> One would prefer to see Ca II diagnostics being developed in terms of qualitative but holistic physics, rather than quantitative but incomplete physics.
>
> LAWRENCE E. CRAM (1983)

Abstract. The bright Ca II H_{2V} and K_{2V} grains, which are intermittently present in the interiors of network cells in quiet-Sun areas, should provide important diagnostics of the dynamical interaction between the quiet photosphere and the chromosphere above it, but their nature has so far eluded identification. We review the extensive observational literature on these grains and on related phenomena. We resolve various contradictions, connect hitherto unconnected observations, distill new constraints and relate signatures in the measurement domain to signatures in the Fourier domain. We then review interpretations and simulation efforts, adding computations of our own to illustrate modeling options. We conclude that the grains are a hydrodynamical phenomenon in which magnetic fields do not play a major role. The grains are due to interference between a pervasive standing oscillation with about a 180 s periodicity and an 8 Mm horizontal wavelength in the chromosphere and the wave trains of the evanescent *p*-mode interference pattern in the upper photosphere. The roles of short-period waves, shock formation and granular piston excitation and the issue of long-lived patterning remain open; we suggest avenues for further research.

1. Introduction

The Ca II H and K resonance lines at 396.85 nm and 393.37 nm are the only resonance lines in cool-star spectra of the dominant ionization stage of an abundant element that are accessible to ground based observation. They are employed to study a surprising variety of solar and stellar properties. A brief inventory:

(i) *Line formation.* The non-dark core and the central doubly-peaked emission reversals which H and K display in solar spectra (Young, 1872; Hale, 1892; Deslandres, 1892; see StJohn, 1910) were a major testing ground of NLTE line formation theory during the sixties (e.g., Jefferies and Thomas, 1960; for further references see Linsky and Avrett, 1970).

(ii) *Partial redistribution.* H and K limb darkening, especially of the H_1 and K_1 minima between core and wings, has played a similar role in the development of partial frequency redistribution formalisms (see Linsky and Avrett, 1970, for earlier references; Vardavas and Cram, 1974; Milkey *et al.*, 1975b; Shine *et al.*, 1975a, b; Ayres, 1975, 1977b; Uitenbroek, 1989b).

[1] Sterrekundig Instituut, NL-3508 TA Utrecht, The Netherlands.
[2] Harvard-Smithsonian Center for Astrophysics, Cambridge, MA 02138, U.S.A.

Solar Physics **134:** 15–71, 1991.

(iii) *Wilson–Bappu effect.* The width of the central H and K emission features serves as a sensitive indicator of cool-star luminosity (Wilson and Bappu, 1957; see Linsky, 1980, for references until 1980; Mattig and Kneer, 1981; Kneer, 1983; Engvold and Marstad, 1983; Oranje, 1983).

(iv) *Magnetic activity.* The spatial patterns and strengths of the H and K emission peaks correlate closely with the presence and amount of magnetic flux on the solar surface (Babcock and Babcock, 1955; Howard, 1959; Leighton, 1959; Skumanich, Smythe, and Frazier, 1975; Skumanich *et al.*, 1984; Schrijver *et al.*, 1989), and therefore, the strength of the excess core emission serves as an informative gauge of magnetic activity in cool stars (e.g., proceedings of the Cambridge Cool Star Workshop series, the Utrecht Ph.D. theses by Middelkoop, 1982; Oranje, 1985; Schrijver, 1986; Rutten, 1987).

(v) *Rotation.* The strength of the excess H and K core emission is rotationally modulated per star, enabling measurement of rotation periods (Vaughan *et al.*, 1981).

(vi) *Flux tubes.* The central H and K emission features provide constraints on 'flux-tube' structure and dynamics (Walton, 1987; Ulmschneider, Muchmore, and Kalkofen, 1987; Solanki, Steiner, and Uitenbroek, 1991).

(vii) *Atmospheric modeling.* The extended H and K line wings are sensitive to the local temperature (Owocki and Auer, 1980) and serve to derive empirical atmospheric models, for the quiet Sun (e.g., Ayres and Linsky, 1976; Ayres, 1977b; Avrett, 1985; Ayres, Testerman, and Brault, 1986), for solar plage (e.g., Shine and Linsky, 1974; Kelch and Linsky, 1978; Lemaire *et al.*, 1981), for solar flares (e.g., Machado, Emslie, and Brown, 1978), and for other stars (e.g., Desikachary and Gray, 1978; Kelch, Linsky, and Worden, 1979). Table 2 of Linsky (1980) gives further references.

(viii) *Granulation.* The fine structure in the outer H and K wings shows the reversal of the granular temperature contrast in the upper photosphere (Evans and Catalano, 1972; Suemoto, Hiei, and Nakagomi, 1987, 1990).

(ix) *Seismology.* The intensity modulation of the inner H and K wings serves as a rich p-mode diagnostic in helioseismology (Duvall *et al.*, 1988; Jefferies *et al.*, 1988), while oscillatory modulation of the central emission peak has been claimed for ε Eri (Noyes *et al.*, 1984).

(x) *Velocity fields.* The large opacity of the H and K wings transforms superimposed weak blends into useful velocity diagnostics by shifting their formation heights over well-defined amounts (Canfield and Musman, 1973; Ayres, 1977a; Gurtovenko, Sheminova, and Rutten, 1985).

(xi) *Limb emission.* Some of the blends in the H and K wings are observed in emission near the solar limb and in stellar spectra and supply diagnostics of NLTE line formation processes (e.g., Canfield, 1971; Cram, Rutten, and Lites, 1980; Watanabe and Steenbock, 1986; see Rutten and Stencel, 1980, for a catalogue).

(xii) *Limb polarization.* Finally, H and K display an interesting pattern in linear polarization near the solar limb to which quantummechanical interference between H and K contributes (Stenflo, Baur, and Elmore, 1980; Stenflo, 1980; Auer, Rees, and Stenflo, 1980).

This rich array of diagnostic applications is not backed by satisfactory understanding of the formation of the solar H and K lines. Although one-dimensional studies have reached a high level of sophistication (e.g., Vernazza, Avrett, and Loeser, 1981; Avrett, 1985; Uitenbroek, 1989b), the fact remains that these lines show much puzzling fine structure, both in their cores and in their wings, with large spatial and temporal variations. There are virtually no locations in quiet areas on the Sun where the spatially-averaged doubly-peaked core profile actually occurs (e.g., Pasachoff, 1970; Grossmann-Doerth, Kneer, and von Uexküll, 1974), so that interpretation of spatially-averaged profiles in terms of plane-parallel models remains questionable. The Wilson–Bappu effect still poses problems, as do the formation of the emission features, the 'basal Ca II flux' (Schrijver, Dobson, and Radick, 1989), the complex H and K oscillation patterns, etc.

In their excellent review of H and K Linsky and Avrett (1970) observed that there were 'three separate literatures growing up in splendid isolation of each other', viz. about plane-parallel explanations of the double reversal, high spatial resolution observations without theoretical interpretation, and the Wilson–Bappu effect. That observation still holds; in the meantime an extensive fourth H and K literature has grown out of stellar magnetic activity, again largely independent of the others, while a fifth literature concerns chromospheric oscillations. In this review we try to link the first, the second and the fifth by concentrating on a specific class of H and K reversal features: the bright H_{2V} and K_{2V} cell grains.

Narrowband spectroheliograms taken in the H and K line cores display a variety of bright features. Fine examples are provided by Hale and Ellerman (1904) and by Title (1966) (plates 5, 12, 13, 22, 40, and 41). Such heliograms show the calcium network outlined by strong emission in clusters of small, bright elements. The latter typically have symmetrical H and K profiles with high double peaks and enhanced line wings. They persist for at least 10 min, probably much longer, and they do not participate in three-min 'chromospheric' oscillations. Similar emission is seen from plages. The network and plage emission patterns are co-spatial with locations of enhanced magnetic field density; it is these components that produce the well-defined correlation between H and K excess line-core flux and magnetic activity of cool stars (Schrijver *et al.*, 1989).

By contrast, the H_{2V} and K_{2V} 'intranetwork bright points' or 'cell flashes', which we call 'cell grains' here, originate exclusively within cell interiors in quiet areas of the solar surface. They show emission primarily in the violet H_{2V} and K_{2V} peaks (see Figure 1 for H and K nomenclature). This is particularly clear on plate 24 of Title (1966) of which Leighton (1961) remarked: "... as the slit scanned the solar surface, we also scanned the slit past the spectral line, so that we obtain a combination spectrogram and spectroheliogram. It has been known for a long time that the K_2 emission is stronger in the *violet* component of the K_2 line. It think we have tracked this down to a difference in the *kinds of features* which produce the emission. We see many sharp, bright points of emission scattered about the disk, and these are more numerous and brighter in the violet component of K_2 than in the red". (This plate is reprinted as Figure 7.9 in Zirin 1988 but in mirror image with respect to the specification in the caption.) Another

remarkable image is the K_{2V} spectroheliogram taken by Gillespie at Kitt Peak, reportedly the best K-line spectroheliogram ever obtained. A large part of this negative forms the cover picture of Lites (1985a); smaller parts have been published by Skumanich *et al.*

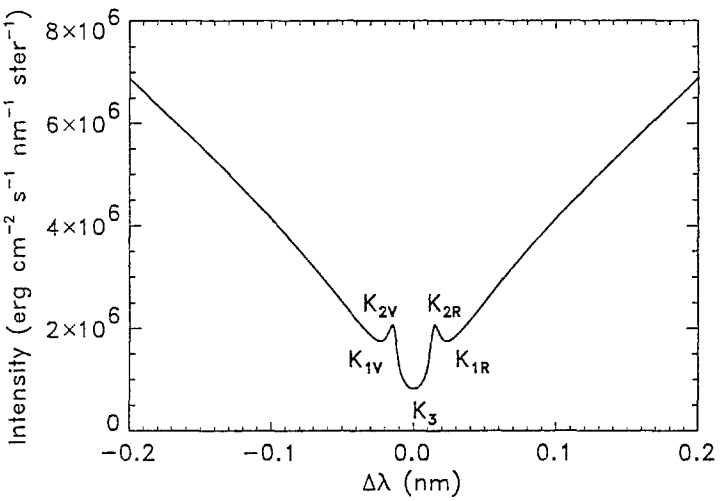

Fig. 1. Theoretical Ca II K profile with standard H and K nomenclature. K_3 denotes the central absorption dip; K_{2V} and K_{2R} the emission peaks on the violet side and the red side of line center; K_{1V} and K_{2V} the dips near $\Delta\lambda = \pm 0.03$ nm from line center.

(1984), Gaizauskas (1985), Lites (1985b) and in positive as Figure 2.9 in Zirin (1988) (with the caption in error in specifying it as line center). Another part of it opens this issue of *Solar Physics* – this is the first high-resolution Ca II frontispiece of this journal.

The H_{2V} and K_{2V} cell grains are small (1.5 Mm or less) and short-lived (100 s or less); they come and go with 2–5 min intervals and they appear to be organised in 5–10 Mm horizontal patterns. They are connected to 'bright threads' and 'dark whiskers' in the inner wings of the H and K lines and to oscillatory phenomena observed in the H and K cores, in the Ca II infrared lines, in Hα and in other lines. They are probably connected with similar bright points seen in the ultraviolet near 160 nm; they are perhaps connected with chromospheric 'jets' observed in ultraviolet C I lines and they are reported to be co-spatial with areas of enhanced magnetic field.

The H_{2V} and K_{2V} cell grains have served no diagnostic purpose as yet, in contrast to the dozen H and K properties listed above. Nevertheless, they attract attention because they represent a specific, well-defined phenomenon which seems to provide direct evidence of wave- or shock-like disturbances that travel upwards in the atmosphere. They should, therefore, represent valuable diagnostics of the dynamical interaction between photosphere and chromosphere in the cell interiors of quiet areas: 'it is conjectured that these (cell grains) provide a direct picture of the processes responsible for a significant part of the nonradiative heating of the quiet chromosphere' (Cram and

Damé, 1983); a direct link between grains and chromospheric heating was recently claimed by Kalkofen (1989). Such claims require substantial evidence, however; so far, there is no definitive interpretation of the observed grain behavior – their nature remains a puzzle.

In this review, we take a hard look at the existing observations to define constraints on cell grain formation. Our starting point is that the spatial, temporal and spectral patterns which the grains display are sufficiently intricate to constrain grain models without presupposing physical mechanisms. This seems a worthwhile approach because no modeling effort has been able to reproduce the observed patterns satisfactorily. Essential ingredients appear to be missing; describing *how* the Sun makes cell grains may bring us closer to the physical *why*.

In Section 2 we review the observations. The pertinent literature is large and contains apparent contradictions. It consists of two distinct and largely independent sets of analyses, addressing (a) event signatures in the spatial and temporal measurement domain or (b) oscillatory properties diagnosed with Fourier transforms. We review both sets, resolve various contradictions, relate them to one another and derive new observational constraints. In Section 3 we summarize previous theoretical work and add schematic computations to illustrate various modeling options. We discuss the nature of cell grains and related phenomena in Section 4 and programs for the future in Section 5.

2. Observations

The cell grain literature started with the observations of Hale and Ellerman (1904) who called them 'minute bright calcium flocculi' to distinguish them from the coarser 'flocculi'. Later, the names 'fine mottles' and 'coarse mottles' were used for the same phenomena (e.g., de Jager, 1959, p. 126). The coarse features coincide with areas of enhanced magnetic field (Babcock and Babcock, 1955; Leighton, 1959; Howard, 1959, 1962) and constitute the calcium network (Deslandres, 1910), which corresponds to the magnetic network and to supergranulation cell boundaries (Simon and Leighton, 1964); they are seen in Hα as elongated features clustered in 'rosettes' (Beckers, 1964).

The smaller features are the subject of this review. They appear on Ca II H and K filtergrams and spectroheliograms as bright roundish dots with sizes of only 1–2 arc sec and occur within cell interiors. They have been called 'bright cell points' or 'intranetwork bright points' in more recent years (e.g., Leighton, 1961; Bappu and Sivaraman, 1971; Liu, Sheeley, and v. P. Smith, 1972; Cram and Damé, 1983; Zirin, 1988), but we prefer to follow the example of Beckers (1964) (his Table 23) and Skumanich *et al.* (1984) by designating them as 'grains' rather than points because they show fine structure at high resolution (Beckers and Artzner, 1974; Cram and Damé, 1983). We make no distinction between the H line and the K line because their properties are virtually identical; we use K as the generic symbol and H for observations taken in the H line.

Jensen and Orrall (1963) and Orrall (1965) were the first to point out that K_{2V} grains are preceded by brightening of the wings of the H and K lines. This is an important point.

The wings originate from the upper photosphere, deeper for larger wavelength separation from line center, so that this observation implies that the K_{2V} grains, which are presumably formed in the low chromosphere, result from something or are connected to something occurring in the photosphere. Since then, their evolution has been studied by Bappu and Sivaraman (1971), Wilson and Evans (1971), Wilson *et al.* (1972), Liu, Sheeley, and van P. Smith (1972), Liu (1974), Beckers and Artzner (1974), Cram (1974), Punetha (1974), Zirin (1974), Cram, Brown, and Beckers (1977), Cram (1978), Duvall, Livingston, and Mahaffey (1980), and Cram and Damé (1983). The most informative of these papers are Cram (1978) and Cram and Damé (1983). They are complementary: the first paper displays K-line structure in the Fourier domain while the later one provides measurement-domain diagnostics of the H line. We discuss these two papers in detail and, therefore, invite the reader to have them at hand while reading this review (as well as a magnifier because the plates and (k, ω) diagrams in the two papers have been printed at too small scales).

2.1. Spatio-temporal domain

Cram and Damé (1983) digitized a 24-min sequence of Ca II H spectrograms taken at 10 s intervals under excellent observing conditions in the Sacramento Peak HIRKHAD program (Beckers *et al.*, 1972). They furnish space-time diagrams of the spatial variation along the 102 Mm slit of various spectral features characterizing the line core as well as time-resolved spectra showing the spectral evolution of the line core and the inner wings for different points on the solar surface, both within network cells and on cell boundaries. One of their time-resolved cell spectra is reprinted on a better scale in Damé (1984), with two sets of tracings depicting the K_{2V} phenomenon.

2.1.1. K_{2V} *Cell Grain Evolution Patterns*

Figure 2 is a sketch after panels 111–120 of Figure 4 of Cram and Damé displaying cell-interior behavior of the H line. We choose a moment at which the line has a dark unshifted K_3 core, no K_{2V} or K_{2R} emission and dark wings as the starting point for our discussion of grain evolution. The subsequent evolution pattern has three distinct aspects – the wing brightening, the K_{2V} flash, and the K_3 line-core Doppler manoeuver.

(i) *The wing brightening.* Brightenings appear symmetrically in the far wings, near $\Delta\lambda \approx 0.3$ nm. They sweep inwards towards the line core, progressing very fast at first with spectral phase speeds of 0.01–0.02 nm s^{-1} (Liu, 1974; Beckers and Artzner, 1974), too fast to give a resolvable phase difference for the 30 s frame rate used by Jensen and Orrall (1963). Closer to line center, the brightenings usually slow down markedly after they pass $\Delta\lambda \approx 0.1$ nm, to an inward progression speed in the spectrum of only 0.5–1 pm s^{-1} (Cram and Damé, 1983, Figure 4). The transitions from dark to bright are distinct, resulting in the appearance of dark branches in the time-resolved spectra of Cram and Damé.

The dark inner-wing features outlined by the brightenings were called 'dark whiskers' by Beckers and Artzner (1974) who studied the HIRKHAD time series of Beckers *et al.* (1972). They describe the same phenomenon in terms of dark whisker contraction,

rather than as bright 'threads' propagating inwards as Liu (1974) did. The two descriptions are complementary. The choice to emphasize the dark rather than the bright features is natural when looking at spatially resolved H and K spectra from cell

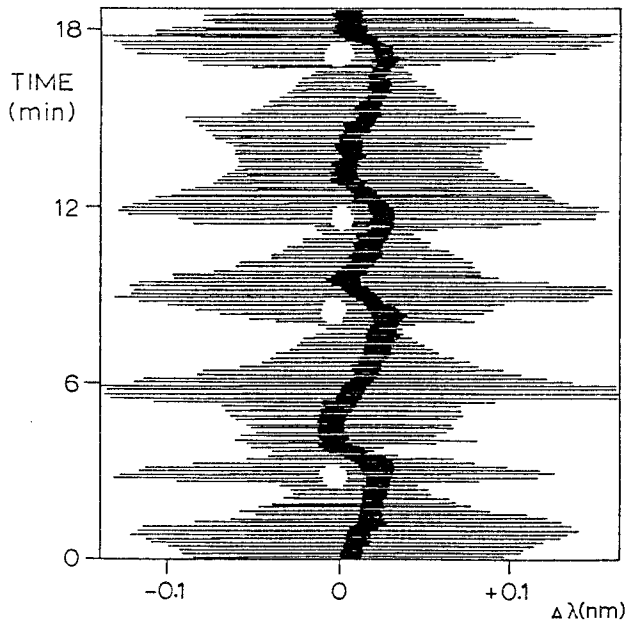

Fig. 2. Sketch of the cell-interior behavior of the intensity in the Ca II K core with time, after Cram and Damé. Time increases upwards; the abscissa specifies wavelength separation from line center at rest. Symmetrical wing brightenings come in from the far wings, fast or instantaneous at first but slowing down near line center. They outline symmetrical 'dark whiskers' which appear as dark branches, with triangular tops. At the same time the dark K_3 core shifts gradually redward. Bright K_{2V} grains flare up when the wing brightenings reach closest to line center; at the same time, the line core reaches maximum redshift. The grains decay quickly while the line core shifts back abruptly, reaching a blueshift that is generally smaller than the maximum redshift. The extended line wings darken abruptly, sometimes at all wavelengths simultaneously. The pattern often repeats a few times, at irregular 2–5 min intervals and with much variation in whisker and grain brightness.

interiors. Particularly fine examples are given by Wilson and Evans (1971) and by Beckers *et al.* (1972). Such spectra show a pronounced pattern of dark whiskers jutting out symmetrically from the H and K line cores. Each whisker ends rather sharply and there is much variation in whisker length along the slit because each whisker is at its own stage of contraction. The visual impression that these sharp, dark extensions from the dark line core make is stronger than the wing brightenings. (The network is seen on such spectrograms as very bright streaks that extend far into the wings.)

The dark branches seen in the time-resolved spectra of Cram and Damé display the time evolution of the dark whiskers. The difference in brightness progression (or dark whisker contraction speed) between the outer and the inner wings produces two distinct stages. The full extent of the whisker modulation of the outer wings is best seen in

Figure 5 of Cram and Damé in which a background profile was subtracted. These time-resolved modulation spectra show a distinct pattern of dark and bright horizontal bars across their full widths (e.g., panel 115). This implies that the outer-wing whisker modulation affects the wings already further out than the time-resolved spectra and our sketch in Figure 2 suggest.

The inner-wing whisker modulation has slower inward progression near line center. This progression is symmetric with regard to the line center at rest and produces conspicuous dark triangles in the time-resolved spectra of Cram and Damé. The triangles point upwards, in the time direction; each top marks the moment at which the wing brightenings reach line center. Figure 4 of Liu (1974) shows that at a given wing wavelength the intensity drops only slowly after the dark-to-bright transition has passed.

(ii) *The* K_{2V} *flash.* There is often a sudden impulsive narrow-band brightening on the violet side of the core at the moment when the dark-to-bright transitions converge at line center, i.e., on the violet side of the top of the dark triangle outlined by the inner-wing whisker modulation. These bright flashes are the K_{2V} grains. The wing brightening always vanishes during the K_{2V} phenomenon, often already before the K_{2V} feature reaches maximum intensity. It often vanishes abruptly, at all wavelengths in the inner wings simultaneously (Figure 5 of Cram and Damé). After some time the next cycle follows, starting with new wing brightenings.

Multiple cycles of this evolutionary pattern produce a sequence of pairs of dark branches in the time-resolved spectra, symmetrically jutting out from line center and a few minutes apart. Their upper parts are triangular; the K_{2V} grains occur besides their tops. Such sequences appear in panels 114–116 and 119–120 of Figure 4 of Cram and Damé, with spatial overlap within these two sets. The other cell-interior panels are relatively empty of H_{2V} grains.

(iii) *The* K_3 *Doppler manoeuver.* The K_3 absorption minimum moves systematically redward while the wing brightening progresses inward. It reaches maximum redshift at the moment of the K_{2V} flash. This maximum redshift is sizable, 5–10 km s^{-1} if converted into velocity (Mein *et al.*, 1987).

Duvall, Livingston, and Mahaffey (1980) claim that this redshift of the K_3 feature is a pseudo-phenomenon resulting from the K_{2V} flashes. The strongest K_{2V} grains indeed extend across the rest wavelength of line center, but there are many examples in the Cram and Damé time-resolved contrast spectra in which H_3 moves steadily redward already during the preceding dark whisker contraction, smoothly continuing when the H_{2V} emission sets in. The K_3 redward shift is a regular and gradual phenomenon and always part of the pattern; this is especially clear in Figure 2 of Damé (1984) and in panels 114 and 115 of Figure 5 of Cram and Damé.

The K_3 core usually shifts back to the violet after the K_{2V} grain occurs, usually simultaneously with the disappearance of the wing brightening. The maximum blueshift is reached quickly, within 10–30 s, and is smaller than the maximum redshift. The line core profile is then reversedly asymmetric, with larger residual intensity in the red flank; sometimes, but rarely, it displays a K_{2R} peak at this moment. After this sudden shift to the blue, the core often starts moving slowly back to the red while new brightenings appear in the wings, in the next cycle.

We have now described the standard evolution pattern of a K_{2V} grain, consisting of the wing brightening which sweeps in symmetrically from the outer wings to reach line center at the moment of the K_{2V} flash, the slow blue-to-red shift of K_3 before the K_{2V} flash and its rapid but smaller subsequent red-to-blue shift, and the K_{2V} flash itself. We refer to this pattern as 'standard', but there is large variation. Figures 4 and 5 of Cram and Damé indicate that the triangular inner-wing whisker contractions always follow on dark outer-wing whiskers but that H_3 redshifts are also present with dark whiskers and without H_{2V} grains. Part of this variation may arise because the components operate at different spatial scales. For example, panel 113 of Figure 4 of Cram and Damé shows two successive dark triangles near its top without H_{2V} flashes, but panels 114 and 115 (adjacent on the Sun) show the same triangles with bright H_{2V} grains; conversely, panel 116 shows large H_3 redshift at one-third from the top without a grain, but an adjacent grain is seen in panels 115 and 114 for the same H_3 excursion. We return to these scale differences below.

A notable property of the standard pattern is its asymmetry in time, with brightness propagating inward from line wings to line center but never outward, and with slow redward but fast blueward K_3 shifts. Duvall, Livingston, and Mahaffey (1980) claim that they observe reversed center-to-wing propagation in the form of $\vee$-shaped patterns in their time-resolved modulation spectrum. Their claim is of obvious interest in the context of vertical energy transport and requires closer scrutiny. Detailed inspection of their time-wavelength diagram shows that the apparent $\vee$ patterns result from the subtraction of the averaged profile from the data. The diagram contains large dark $>$ shapes and smaller dark $<$ shapes of which the lower arms (decreasing $\Delta\lambda$ from line center) make up a $\wedge$ pattern; it corresponds to the triangular pairs of dark branches discussed above. Its blue arms are enhanced because subtracting the time-averaged profile darkens K_{2V} more than K_{2R}. The off-center tip of this $\wedge$ consists of the dark redshifted K_3 core; the short apparent $\vee$ pattern which follows is caused by the subsequent blueshift of the K_3 dip. The $\vee$ is also enhanced by the subtraction and it has no arms that reach out into the wings. These observations actually fit the standard pattern quite well, indicating that Duvall, Livingston, and Mahaffey indeed observed a cell interior. They averaged the spatial information along their 5.5 Mm slit; their diagram contains evidence of phase mixing between two independent K_{2V} sequences. We conclude that there is no contradiction with the standard pattern from the Cram and Damé data and that there is no indication of reverse propagation in either set.

2.1.2. K_{2V} *Cell Grain Space-Time Patterns*

The number of contiguous frames in Figure 4 of Cram and Damé showing the same feature is typically 1–2 for H_{2V} grains, corresponding to about 1–2 Mm extent. The dark whiskers and H_3 Doppler excursions seem to extend over 2–3 adjacent frames but this is more difficult to ascertain. The spatial and temporal patterns are better discerned in the six space-time diagrams in Figure 3 of Cram and Damé, to which we turn now. They fall into two distinct groups:

(i) *The* H_{2V}, H_{2R}, *and* H_3 *intensity diagrams and the* H-*index diagram.* The three

line-core intensity diagrams, of which the H-index diagram represents a weighted mean, are mostly dark in cell interiors. The network appears as bright, slightly slanted striping. They contain small bright grains which are numerous only in the H_{2V} diagram.

(ii) *The* H-*wing intensity diagram and the V/R diagram.* The first diagram shows the space-time behavior of the outer-wing intensity modulation at $\Delta\lambda = -0.14$ nm from line center; the second diagram displays the ratio of the H_{2V} and H_{2R} intensities. These two diagrams differ markedly from the other four and also between each other. They show equal amounts of dark and bright, alternating in modulation patterns. The network appears as bright striping (H-wing diagram) or as pattern erasure (V/R diagram).

The whisker scale is best shown by the H-wing diagram. It shows narrow vertical columns with dark and bright modulation. It is remarkably similar to 'time-slice diagrams' of the solar granulation which portray granular evolution by showing the temporal behavior of the intensity along a linear cut across the solar surface on successive images. Such granulation diagrams represent a wide-band filtergram analogous to these space-time diagrams derived from spectra. Their appearance is nearly the same in the pattern, apart from the absence of bright network striping; however, detailed comparison (with an unpublished granulation time-slice diagram, courtesy of P. N. Brandt) shows that the H-wing structure is spatially about twice as coarse while the temporal modulation is about twice as fast as for the granulation. The widths of the vertical columns in the H-wing diagram are about 2–3 Mm, in accordance with the remark by Beckers and Artzner (1974) that dark whiskers are typically a few arc sec wide. This scale is indeed twice that of granulation, which implies that the H and K wing whiskers should not be identified with the granulation modulation observed at larger separation from line center (Evans and Catalano, 1972; Suemoto, Hiei, and Nakayomi, 1987, 1990) which has a spatial anticorrelation between the contrast in the far wings ($\Delta\lambda > 0.3$ nm) and in the inner wings, attributed to the contrast reversal above granules (e.g., Holweger and Kneer, 1989). This anticorrelation holds only for granular scales; Suemoto, Hiei, and Nakagomi (1990) obtain it after spatial filtering to get rid of larger modulation with about 2.5 arc sec wavelength, i.e., of the whiskers discussed here. Thus, the intensity variations in the outer wings of H and K represent a mixture of reversed granulation contrast and of wing whiskers. Figure 1 of Suemoto, Hiei, and Nakagomi (1990) displays raw data before spatial filtering; it shows that the whisker modulation gains dominance towards line center.

The three line-core intensity diagrams (H_{2V}, H_3, and H_{2R}) show dark blobs of larger dimension, with widths of about 3–5 Mm; they are most clearly evident in H_3. Cram and Damé presume that these correspond to the 'dark clouds' found in cell interiors (Bappu and Sivaraman, 1971; Zirin, 1974), which are dark, roundish features observed on K_3 heliograms and filtergrams (e.g., Plate II of Hale and Ellerman, 1904). Bappu and Sivaraman specify sizes of 4–6 Mm, Zirin a horizontal extent of about 10 Mm and a height of 3–4 Mm. Bappu and Sivaraman (1971) and Sivaraman (1982) attribute these dark features to 'condensations' that supposedly fall down with 5–8 km s^{-1} velocity. There are indeed many dark elements at the same time and location in the H_3 and H_{2R} space-time diagrams, implying redshifts; however, a closer inspection using overlays

shows that many of these are also present in the H_{2V} diagram. In addition, comparing the H-index diagram to the H-wing diagram shows close correspondence between the bright and dark space-time patterns in these two diagrams, indicating that much of the dark structure is due not to H_3 Doppler behavior but to intensity modulation which affects the wings as well, i.e., to the dark whiskers seen in the spectra. Their change from elongated shape in the H-wing diagram to roundish in the line-core diagrams corresponds to a doubling in size; in high-resolution spectra such as the one published by Beckers *et al.* (1972) this can be seen as the widening of some dark whiskers near line center noted by Beckers and Artzner (1974). This correspondence between the line wing diagram and the line core diagrams confirms that the outer-wing whisker modulation and the inner-wing whisker modulation tend to act together.

The H_{2V} cell grains are, of course, best seen in the H_{2V} diagram. It is peppered with small features, both dark and bright, in addition to the whisker pattern. Some of the features are very bright; these are the grains. The brightest grains flow over into line center and appear also in the H_3 and H-index diagrams: all bright grains in the H_3 diagram correspond one-to-one with very bright H_{2V} grains. (They might be less visible if the real minimum intensity, i.e., of the shifted H_3 core itself, were plotted instead of the intensity at the fixed rest wavelength of line center.)

Beckers and Artzner (1974) remark that K_{2V} grains often have spatial structure which differs from the preceding dark whisker: the K_{2V} grains are smaller, and often show multiple structure. Cram and Damé also observe fine-scale structure in several H_{2V} grains, but they stress that nevertheless the H_{2V} grains invariably appear as localized intensity maxima in a brightness pattern of larger scale. The latter fills the H_{2V} diagram (for cell interiors) with dark and greyish areas that alternate both in space and time in oscillatory fashion; the H_{2V} grains appear in some of the latter but not regularly so – there are many grey locations without bright grains. The H_{2R} diagram shows a similar distribution of grey locations but far fewer bright grains, of which none corresponds to bright grains in H_3. Some lie close to grains in the H_{2V} diagram but most do not.

Let us now turn to the V/R space-time diagram of Cram and Damé. It differs strikingly from the other diagrams. It resembles the H-wing diagram in the sense that black and white are about equally present with oscillatory characteristics, but it has coarser spatial and faster temporal modulation. It is also much more regular, with less independence between adjacent columns: in some areas it contains wavy structures made up of dark and bright patches of 2–5 Mm size and 1 min duration in very regular juxtaposition, which implies horizontal phase propagation with extended spatial coherency. It is the *only* diagram in which the H-wing intensity patterns are absent. This confirms that the whisker intensities are about equal in H_{2V} and H_{2R}; normalizing H_{2V} intensity by H_{2R} intensity fully cancels the whisker modulation which is so prominent in all line-core diagrams. Since the V/R ratio exceeds unity (bright in the diagram) for bright H_{2V} and/or dark H_{2R} and, conversely, is less than unity (dark) for dark H_{2V} and/or bright H_{2V}, bright and dark V/R corresponds to redshift and blueshift of the dark H_3 core, respectively. The V/R diagram obviously exhibits primarily the signature of oscillatory behavior; we infer that it displays H_3 Doppler manoeuvers and their spatio-temporal

properties. This implies that the H_3 core oscillates regularly with 2–4 min periodicity and 4–10 Mm wavelength, in patterns with much horizontal phase propagation and coherence. We return to this behavior in the next section.

How do these diagrams tie together? Overlaying the H_{2V} diagram with a transparency of the V/R diagram shows that all grey areas of the former are bright in the latter: the V/R diagram marks not only the actual grain sites but *all* space-time locations where a grain *might* occur. These are the sites where H_3 has appreciable redshift. Overlaying the V/R diagram with the H-wing diagram demonstrates that these are not necessarily sites of bright outer-wing whiskers: the H_3 Doppler oscillation seen in the V/R diagram is not closely cospatial or cotemporal with the whisker intensity modulation pattern of the H-wing diagram. Overlaying all three diagrams together shows that H_{2V} *cell grains occur exclusively when and where both the* V/R *diagram and the* H*-wing diagram are bright.* Moreover, this triple overlay suggests that H_{2V} grains occur preferentially at the end of the outer-wing brightening, and that fine structure in the grains arises also from interference between the V/R pattern and the smaller-scale H-wing pattern.

We conclude that the H_{2V} diagram is a mixture of whisker modulation and H_3 Doppler shift, while the other two line-core diagrams show primarily the whisker modulation. Both the whisker modulation and the H_3 Doppler excursions are oscillatory in character, but with different spatio-temporal patterns; these are best separated in the H-wing and V/R diagrams, respectively. H_{2V} cell grains are produced by coincidence of H_3 redshift and a bright whisker, in agreement with the standard pattern exhibited by the time-resolved spectra. The selective occurrence of cell grains arises from pattern difference between the two oscillations.

Similar overlaying of the H-wing and V/R diagrams with the H_{2R} diagram indicates that the few H_{2R} grains which are present occur only when the H-wing diagram is bright while the V/R diagram is dark. One would expect the latter, of course, since dividing by larger R intensity decreases the V/R ratio; however, these dark features are invariably part of the wavy structures in the V/R diagram, falling in place beside dark features that are not produced by bright H_{2R}. Thus, H_{2R} grains seem to obey the inverse rule and to occur where and when H_3 is blueshifted while the whisker is bright.

The paucity of H_{2R} grains compared to H_{2V} grains implies that the condition of bright whisker plus H_3 blueshift is less frequently fulfilled than the co-occurrence of bright whisker plus H_3 redshift. This suggests that the two oscillation patterns are not independent. It is not easy to gauge this by overlaying the H-wing and V/R diagrams: in some places they have sufficient similarity to suspect pattern correlation, but in other places they appear wholly different.

2.1.3. K_{2V} *Cell Grain Oscillation Patterns*

We postpone discussing Fourier analyses to Section 2.2; here we discuss the oscillatory signatures of cell grains in the spatio-temporal domain. Whiskers and K_{2V} grains tend to repeat in time, at intervals which vary from two to five minutes and with large diversity in occurrence and pattern. The average period is about 180 s (Jensen and Orrall, 1963; Noyes and Leighton, 1963; Liu, 1974; Beckers and Artzner, 1974; Punetha, 1974; Mein

and Mein, 1976; Cram, Brown, and Beckers, 1977; Duvall, Livingston, and Mahaffey, 1980; Damé, Gouttebroze, and Malherbe, 1984; Damé and Martić, 1987). The length of a typical oscillation train seems short. Beckers (1964) determined 4 min duration from blink comparison of a sequence of K-line spectroheliograms taken at 2–3 min intervals, which indicates that the grains oscillate for only one or two cycles. Liu, Sheeley, and v. P. Smith (1972) remark that only some of the grains recur but the examples of Liu (1974) indicate wavetrains of up to 5 peaks, as do some time-resolved spectra of Cram and Damé. Our discussion of the Cram and Damé space-time diagrams above indicates that grain repetition is set by spatio-temporal phase coincidence between the K_3 Doppler oscillation and the K-wing brightness modulation; we therefore discuss the space-time signatures of these two patterns in more detail.

Cram and Damé's V/R diagram shows H_3 Doppler behavior, bright for redshift and dark for blueshift. Cram and Damé remark that the V/R ratio often changes rapidly, with asymmetry in the sense that points with $V/R > 1$ change more rapidly to $V/R < 1$ than conversely; this corresponds to the faster blueward than redward H_3 Doppler manoeuvers seen in their time-resolved spectra. A vertical cut at a given location along the slit reproduces the standard pattern, with the slow H_3 progression to the red here seen as slow brightening and the faster subsequent shift to the blue as a rapid darkening, one cycle taking 2–4 min. A horizontal cut at a given moment produces intensity variations with about 8 Mm spatial periodicity along the slit.

The V/R diagram displays phase coherency especially at lower left in the diagram where the wavy structure is most pronounced. It has 2 min periodicity, a spatial extent of at least 10–15 Mm and a lifetime of two or more full cycles; it seems even to extend across cell boundaries (the network shows up in the V/R diagram as grey vertical striping because it produces doubly-peaked H profiles without V/R asymmetry and with slower time variations). The slanted linear structures of these patterns imply phase progression along the slit; we measure typical phase velocities of 60 km s^{-1} and higher. Such coherency patterns may produce apparent horizontal motions in narrow-band K_3 filtergram sequences, dark patches appearing alternatively at two adjacent sites. Zirin (1974) observed 'violent horizontal oscillations' of K_3 clouds in successive filtergrams; we suspect that, rather, he saw such phase patterns. Zirin's values for the horizontal velocities (10 Mm displacement in 3–4 min) correspond to 40–60 km s^{-1} phase velocity, in good agreement with our value above and with the observation by Wilson and Evans (1971) of an apparent phase velocity of 50–100 km s^{-1} from two features seen to separate along their slit. Also Liu, Sheeley, and v. P. Smith (1972) remark that often neighbouring K_{2V} grains seem to go off in succession, 'giving the erroneous impression of rapid proper motions with speeds on the order of 100 km s^{-1}', while Wilson *et al.* (1972) conclude that the spatial stability of K_{2V} grains is better than 1–2 arc sec over 4 min.

Let us now turn to the H and K wing modulation pattern. The H-wing diagram of Cram and Damé shows oscillatory behavior but with longer periods than the V/R diagram, in agreement with the earlier results of Jensen and Orrall (1963) and Noyes and Leighton (1963) that K_3 oscillates at 170 s and the K wing at about 250 s. The

oscillatory signal is less clean than in the V/R diagram; there seems to be mixing of modulation of about 5 min periodicity and about 5 arc sec extent and modulation by faster and smaller-scale variations. Some features are narrow at long duration and may be due to (reversed) granulation. Phase coherency is not clearly evident in this diagram.

The network stands out in this diagram as bright striping, due to the brightening of the H and K wings in magnetic elements. Liu and Sheeley (1971) ingenuously placed a photocell behind a hole in their movie projection screen and so traced the temporal behavior of various features on a time-lapse sequence of K_{2V} spectroheliograms. They found that the 170 s periodicity must be attributed to cell interiors and has much variation, whereas the network boundaries oscillate regularly at 300 s in K_{2V}. The bright network striping in the H-wing diagram indeed shows slower variations than the cell-interior brightness.

Additional information on the whisker oscillation is available from Doppler shift measurements of Fe I blends in the K-line wings and the Ca II 854.2 nm line (Jensen and Orrall, 1963; Orrall, 1965; Liu, 1974; Beckers and Artzner, 1974; Cram, 1974; Cram, Brown, and Beckers, 1977). In all studies, the spatially-averaged line center in each spectrogram is adopted as line-center rest wavelength, but StJohn (1910) found already that the spatially-averaged K_3 core has a redshift of 1.1 km s^{-1} (cf. White and Livingston, 1981). It presumably results from the standard pattern described above; Sivaraman (1982) quotes it as evidence for the downflow of the K_3 dark clouds. Similar systematic offsets may be present in other lines formed at large heights so that a measured blueshift may actually represent matter at rest (cf. Rottman *et al.*, 1990; Samain, 1991). Differential phase and evolution patterns are not affected unless the spatial averaging per spectrogram is insufficient to reach stability.

Jensen and Orrall (1963) show Doppler shifts of the weak Fe I 393.73 nm blend and of various K-line features. Most of their diagrams concern network features, as is clear from the presence of simultaneous K_{2V} and K_{2R} peaks in their Figure 1, but there are K_{2V} grains in the lefthand panel of their Figure 4 at 10 and 20 min. The Fe I 393.73 nm line in these frames shows no special behavior, just five-min oscillation. The same holds for the Fe I 393.11 nm blend which also exhibits normal five-min oscillation, uncorrelated to the K_2 intensity (Orrall, 1965). Thus, the K_{2V} phenomenon does not possess a clear Doppler signature in the photosphere.

Similar measurements of Doppler shifts related to K_{2V} grains have been made for stronger lines by Liu (1974), Beckers and Artzner (1974), Cram (1974), and Cram, Brown, and Beckers (1977). Liu (1974) shows an example (his Figure 4) in which the redshift of the stronger Fe I 391.03 nm line increases with the dark whisker contraction and peaks about 20 s before the wing brightening passes K_1. The shift passes zero at the moment of maximum K_{2V} intensity 1 min later, and continues to the blue to reach 1.0 km s^{-1} blueshift about 30 s later. This behavior is described as standard by Beckers and Artzner (1974) who measured Doppler shifts of the same Fe I 391.03 nm line and the Ca II 854.2 nm line. They give a typical evolution pattern in terms of 'best dark whisker visibility'; transcribing their Table II in terms of brightening reproduces Liu's pattern: maximum redshifts occur shortly before the wing brightening reaches K_1, about

a minute before the K_{2V} grain itself; maximum blueshifts are reached about 50 s after the K_{2V} grain.

Cram (1974) determined redshifts of the Ca II 854.2 nm line simultaneously with K-line behavior from another HIRKHAD data set. Some of his features (tracings 2 and 3) exhibit simultaneous K_{2V} and K_{2R} emission peaks, suggesting that these were network rather than intranetwork features; his tracing 4 displays K_{2V} behavior, with a K_{2R} peak 50 s after the K_{2V} grain. Such K_{2V} peaks are rare but not abnormal and not as unique as Durrant, Grossmann-Doerth, and Kneer (1976) state (cf. Liu and v. P. Smith, 1972). Cram finds that the Ca II 854.2 nm line is unshifted at the occurrence of a K_{2V} grain. The same holds for the K_{2V} event specified in Table 3 of Cram, Brown, and Beckers (1977), who measured phase differences for 7 simultaneously exposed HIRKHAD lines and find that the Ca II 854.2 nm profile reaches maximum redshift 45 s before the K_{2V} grain and maximum blueshift 50 s after it. Similar Doppler behavior is shown by their other lines (Na I D_2, Fe I 393.03 nm, Fe I 393.26 nm, Ni I 589.29 nm), with an indication that weaker lines reach their maximum redshift earlier.

Finally, it is a pity that Cram and Damé have not measured intensities and Doppler shifts for the Ca II 854.2 nm line because their HIRKHAD sequence seems the best of all. Their time-resolved spectra (their Figures 4 and 5) show the strong Fe I 396.93 nm line just inside the right-hand frame edge. The line typically undergoes a marked excursion to the red before the H_{2V} grain and reverts into a smaller blue excursion during the H_{2V} grain.

Together, these spectroscopic event descriptions furnish a rather consistent pattern in which all lines participate with oscillatory Doppler behavior in the whisker oscillation, perhaps with weaker lines leading stronger ones (cf. Durrant, Grossmann-Doerth, and Kneer, 1976). Such single-event descriptions do not supply sufficient statistics for reliable phase and coherency determinations; obviously, that requires Fourier diagnostics which we discuss in Section 2.2. However, space-time event morphology is useful to portray relationships; in particular, Cram, Brown, and Beckers (1977) show instances where the occurrence of a bright granule seems to be a precursor first to a blueshift and then to a burst of 2-min oscillations of K_3 and Hα.

We now turn to the spatio-temporal characteristics of these oscillations as measured on narrow-band K-line filtergrams. Damé and coworkers have analysed two filtergram sequences taken at Sacramento Peak, respectively centered on K_3 (Damé, 1984; Damé, Gouttebroze, and Malherbe, 1984; Gouttebroze, Damé, and Malherbe, 1984; Damé, 1985a; Damé and Martić, 1988) and on K_{2V} (Damé, 1985b; Damé and Martić, 1987). The filtergram bandwidths were 0.12 nm for the K_3 series and 0.06 nm for the K_{2V} series. The first is wider than for the H-index diagram of Cram and Damé so that the first series displays whisker brightness modulation primarily; the second series emphasizes K_{2V} intensity behavior more and therefore mixes in more signal from the K_3 Doppler oscillation.

The K_3 series shows that the cell interior K-core brightness oscillates primarily with about 3-min periodicity while network boundaries oscillate more slowly (Damé, Gouttebroze, and Malherbe, 1984), confirming the work of Liu and Sheeley (1971) and

others and in good agreement with the scales of the whisker modulation in the H-index diagram of Cram and Damé. The K_{2V} series shows that the 3-min oscillation has a preferred spatial wavelength of 8 Mm which is best seen in the phase study of Damé and Martić (1987). They first display spatial phase coherency diagrams for oscillations of specific periodicity, then Fourier-analyse these to derive spatial wavelengths for the coherency patterns. Their phase diagram (their Figure 1(b)) indicates that this 8 Mm 3-min oscillation occurs everywhere, even though its amplitude varies strongly from place to place as illustrated by Figure 3(c) of Damé, Gouttebroze, and Malherbe (1984). This result confirms the scales and coherency patterns seen in the V/R diagram of Cram and Damé.

2.1.4. *Cell Grains in Other Lines*

K_{2V} grains may leave signatures in other spectral lines, but information from such complementary diagnostics is scarce. A few candidates:

(i) *Ca II IR lines.* Cram, Brown, and Beckers (1977) specify that Ca II 854.2 nm brightens in phase with the K_{2V} grain in their Table 3, which implies that the intensity of this line responds to the same layer as K_2, in agreement with the opacities of these features. The velocity behavior of this line is discussed above; the line reaches maximum redshift a quarter cycle before the occurrence of the K_{2V} grain. Deubner and Fleck (1990) display a sequence of Ca II 854.2 nm velocity oscillations in their Figure 3. The amplitude reaches ± 4 km s^{-1} and the excursions are nearly sinusoidal with only a slight hint of sawtooth asymmetry, less than the sawtooth behavior seen for the strong Fe I 396.93 nm blend in Figure 4 of Cram and Damé.

(ii) *Mg II* h *and* k. The resonance lines of Mg II are so similar to H and K that the cell grain phenomenon undoubtedly affects them as well; they may provide additional information thanks to their larger opacity. However, there are no detailed k_{2V} studies available. The whole-Sun k-line filtergram published and correlated with a Ca II K spectroheliogram by Fredga (1971) has insufficient resolution (4 arc sec) to show cell grains. The LPSP experiment onboard OSO-8 had 1 arc sec resolution in one direction; the preliminary results given by Bonnet *et al.* (1978) contain an example of concurrent 200 s oscillations in K and k (their Figure 13) with cell grain behavior in k_{2V} and k_{2R} (their Figures 14 and 15). They obtained a broad set of observations and remark that the wave trains generally last no longer than a few cycles, with periods ranging from 250 s down to 130 s. However, further analyses have not been published, nor are there h and k grain analyses from the more recent data taken with the UVSP instrument on board the Solar Maximum Mission.

(iii) *Mg I* b. November (1989) finds that the surface intensity distribution of the Mg I b_1 line at 517.3 nm, time-averaged over a 190 min sequence, is correlated with persistent horizontal flows measured from the proper motions of individual granules. The line is dark above the divergence centers of the mesogranular pattern in these flows. This correlation implies a link between long-lived intensity modulation at the height of formation of the Mg I b_1 line and subsurface convective flow patterns which should also

exist for the wings or cores of the H and K lines. The mesogranulation cells measure about 5–10 Mm (November *et al.*, 1981) or 4–6 Mm (Brandt *et al.*, 1989); these scales correspond closer to the larger elements seen in the space-time diagrams of Cram and Damé for the H core (dark clouds in the H_2 and H_3 diagrams, oscillation elements in the V/R diagram) than to the smaller scales of the H-wing diagram.

(iv) Hα. Beckers (1964) observed small roundish unresolved dark features in Hα – 0.05 nm which he called grains. They appear all over the disk, also in cell interiors, and Beckers thought it likely that these are identical to the bright K_{2V} cell grains. Bhatnagar and Tanaka (1972) measured the temporal behavior of various spatial elements of 2 arc sec diameter on Hα – 0.05 nm movies, using Sheeley's hole-in-screen technique. They found oscillations of various periodicity, confirming the K-line results of Liu and Sheeley (1971) for Hα: 170 $\pm$ 44 s oscillations in cell interiors, 300 $\pm$ 50 s oscillations in plages and network rosettes. Giovanelli (1974) studied cell-interior Hα features on line center, $\Delta\lambda = \pm 0.025$ nm, $\Delta\lambda = \pm 0.050$ nm, and $\Delta\lambda = \pm 0.075$ nm filtergrams, calling them 'chromospheric granulation'. He found that the contrast reverses between the opposite wings, that it is larger in the blue than in the red wing and that it mostly results from Doppler shifts due to vertical motions. With velocity subtractions Giovanelli (1975) confirmed this oscillatory behavior, finding that the periods are 2.5 min and longer and that maximum downward velocity typically leads maximum intensity by a quarter period.

Kneer and von Uexküll (1986) show a sequence of successive Hα profiles for a cell interior location. The line-center behavior is masked by ratioing to an average profile but this ratioing helps to bring out the inner wing modulation near $\Delta\lambda = \pm 0.05$ nm, which displays 150–300 s periodicity. The red and blue side are indeed in antiphase and the behavior is symmetric and sinusoidal. The velocity amplitudes are about 1 km s^{-1}. The smallness of this value and the sinusoidal character of the oscillation make it likely that this velocity oscillation corresponds to the whisker modulation of the K-wings, not to the sawtooth K_3 motion.

Gaizauskas (1985) displays both a high resolution Hα – 0.06 nm filtergam (his Figure 6(b), positive) and a high-resolution K_{2V} heliogram (his Figure 5, negative). Both show tiny roundish features within the cells and larger and more elongated structures making up the network. The two pictures are so similar in appearance that they strongly suggest that dark Hα – 0.06 nm and bright K_{2V} cell grains belong to the same phenomenon. The contrast reversal agrees with the result of Schoolman (1972) that Hα darkens for temperature increase. However, direct identification has not been made.

(v) Lα. Artzner *et al.* (1978) reported evidence that the central reversal of Lα is appreciably redshifted when the Mg II and Ca II V/R asymmetry ratio are largest. This observation indicates that Lα may behave like K_3 in the standard pattern. The Lα filtergrams taken with the TRC rocket filtergraph (Bonnet *et al.*, 1980, 1982; Foing, Bonnet, and Bruner, 1986) do not show grains in cell interiors; narrow-band K_3 heliograms do not show many cell-interior grains either.

(vi) *The* CN *bandhead.* The only report of simultaneous imaging in K_{2V} and another line that we have found is the time-lapse sequence of spectroheliograms taken in K_{2V}

and the CN 388.3 nm bandhead by Liu and Sheeley (1971). Inspection of their heliogram pair indicates that bright K_{2V} grains are also bright in the CN bandhead. The two images differ much in detail, however. The CN image is finer-featured and contains more bright cell points of weaker intensity. It probably shows the whisker intensity modulation, similarly to the inner wings of H and K. This is also indicated by the Fourier analysis of Kneer, Newkirk, and von Uexküll (1982) who find normal *p*-mode oscillation signatures in CN bandhead power spectra.

(vii) *Infrared* CO *lines*. Ayres, Testerman, and Brault (1986) have obtained simultaneous spectra of infrared CO bands and the K line. These contribute strong evidence to Ayres' proposal that temperature bifurcation splits the atmosphere in hot and cool regions (Ayres, 1981, 1990a, b; Ayres and Wiedemann, 1989; Ayres and Brault, 1990; Athay and Dere, 1990). Ayres seeks his 'cool clouds' in cell interiors in layers near the temperature minimum, and so they might be seen also in H and K.

Athay and Dere (1990) conclude from an analysis of HRTS data that the chromospheric temperature rise is present over 90% of the solar surface and that the remaining 10% may be due to cool clouds of about 2.5 arc sec diameter that are located in cell interiors. This result contradicts the large cool-cloud filling factor derived earlier by Ayres and coworkers; however, Ayres (1990a) now submits that either the clouds are large and fill most quiet-Sun area in a chromospheric layer above the temperature minimum, or that they are small and are located below the temperature minimum with small horizontal filling factor.

Since the whisker brightness modulation and the K_3 Doppler oscillation fully cover cell interiors horizontally and since the K wings and core cover the upper photosphere and low chromosphere vertically in formation, the question arises how to accommodate cool matter within these two oscillation patterns. No identification has yet been made; Lites (1985b) points out that there is no hint of a cool component in the high-resolution H-line spectrogram printed in his Figure 4.

2.1.5. *Bright Points in the Ultraviolet*

Pictures of the Sun taken in the continuum at 160 nm look similar to K_{2V} spectroheliograms, with a grainy but relatively steady network and tiny bright intranetwork 'cell points' which come and go with 1-min lifetimes. Although there are no simultaneous observations to tie the latter directly to K_{2V} grains, their characteristics are so similar that they probably mark the same phenomenon.

The 160 nm bright cell points have been observed with the HRTS rocket spectrograph (Brueckner, 1980; Cook, Brueckner, and Bartoe, 1983) and the TRC rocket filtergraph (Bonnet *et al.*, 1982; Foing and Bonnet, 1984a, b; Foing, Bonnet, and Bruner, 1986; Damé *et al.*, 1986). Like the K_{2V} grains, they are about 1 Mm in size (Cook *et al.*, 1983; Foing and Bonnet, 1984a), persist for about a minute (Cook, Brueckner, and Bartoe, 1983) and have a surface density of 10–20 grains per cell at any given moment. The 160 nm cell points are a continuum feature and can therefore probably be interpreted as local source function enhancements without ambiguity from Doppler shifts. The corresponding variation in brightness temperature is about 50–100 K (Foing and Bonnet, 1984b).

In their initial paper on the second TRC flight, Bonnet *et al.* (1982) claim to see occasional large-scale spatial ordering of 160 nm bright points in wave patterns which consist of ripples that are about 5 Mm apart and reach lengths of 100 Mm, far exceeding typical network cell sizes. We are unable to discern these waves on their best picture (their Figure 6); they are not mentioned again in the subsequent analyses of the same TRC-2 picture by Foing and Bonnet (1984a, b) while Foing, Bonnet, and Bruner (1986) found no such waves in TRC-3 data. Also Cook, Brueckner, and Bartoe (1983) see no evidence of large-scale coherence, but they do find a few instances in which cell points brighten simultaneously over a 20 arc sec field.

Foing and Bonnet (1984a) find Fourier evidence for a pervasive spatial periodicity with 8 Mm wavelength. This was confirmed by Martić and Damé (1989) who analysed a 4.5 min time series of TRC-4 filtergrams taken with a bandpass around 156 nm which contains strong C IV lines. These do not show marked bright cell points (Figure 4 of Damé *et al.*, 1986), but they do have weaker cell-interior intensity modulation in an oscillatory pattern, again with 180 s periodicity, 8 Mm spatial wavelength and present all over the surface. Obviously, longer filtergram time series than the few minutes available from rocket flights are needed to confirm such coherency patterns with more confidence; nevertheless, the rocket data indicate that the 160 nm cell points fully share in the 8 Mm and 3-min oscillatory behavior with large-scale coherence displayed by the V/R diagram of Cram and Damé and the K-line filtergram sequences of Damé and coworkers.

Foing and Bonnet (1984a) show a plot of the intensity across a cell (their Figure 2) which indicates that the bright points share in the 8 Mm modulation: the points are brightest where the slow modulation is bright. The TRC-2 picture (their Figure 2, printed larger as Figure 4 of Foing and Bonnet, 1984b) indeed indicates that the bright points are clustered in clumps with larger dark areas in between; comparing this image with Gillespie's K_{2V} spectroheliogram suggests that the K_{2V} grains possess similar 'mesoscale' clustering if observed at sufficient spatial and spectral resolution. Foing and Bonnet (1984a) derive an average bright-point separation of only 1.4 Mm, but their Fourier methods mix the cell points with the much more closely packed bright points of the network boundaries and plages; their optically-filtered Figure 6 confirms, although there is speckle noise as well, that cell points of small dimension are often organised in tight clusters.

Another 160 nm phenomenon of interest is the existence of the 'chromospheric jets' in C I lines observed with the HRTS spectrograph (Dere, Bartoe, and Brueckner, 1983, 1986). These are bright emission features observed in the three C I lines near 156 nm. They are blueshifted by 10–20 km s^{-1}, their size is about 1 arc sec, they are observed mainly from cell interiors, they occur at 3–5 Mm separations and they live about 50 s. Similar redshifted C I features are also observed, but weaker and much less frequent. Dere, Bartoe, and Brueckner (1983) suggested that the jets may correspond to spicules, but Dere, Bartoe, and Brueckner (1986) propose that the jets, the 160 nm cell points and the Ca II grains are all aspects of the same phenomenon, stating that 'at present, there is little data to decide this question' which remains the case. The temporal

evolution of the jets is yet unknown; there are no simultaneous observations from which their co-occurrence with K_{2V} grains can be tested, nor is their relation to bright points in the UV continuum clear.

2.1.6. *Cell Grains and Magnetic Fields*

An important issue is whether a relation exists between K_{2V} grains and the presence of local magnetic field concentrations ('flux tubes'). Cram and Damé's finding that 'the H_{2V} cell grains invariably appear as localized intensity maxima in the more diffuse brightness maxima of the 3–5 min oscillations' has led Damé and coworkers to propose that magnetic flux tubes concentrate the oscillatory energy present in a more extended wavefront and dissipate it in this point-like appearance (Damé, Gouttebroze, and Malherbe, 1984; Damé, 1985b; Damé and Martić, 1987, 1988).

Damé (1985a) states that a movie of his 52 min sequence of K_3 filtergrams leaves the impression that bright K_{2V} grains appear and reappear at fixed positions 'while a larger size oscillation intensity bulk is passing through', but he provides no measurements of grain location stability. He quotes the frequency recurrence maps of Damé, Gouttebroze, and Malherbe (1984) for this sequence as evidence, but these show primarily H-index-like whisker behavior, and the time average over the whole sequence (their Figure 2(b)) shows no cell grains at all.

A shorter grain location memory is indeed indicated by Figure 4 of Cram and Damé in which some frames (e.g. 115) show sequences of grains while others (113) have none. These sequences cover 2–4 cycles, with much brightness variation between successive flashes; the sequence is too short to provide evidence of longer location stability. Wilson *et al.* (1972) measured the spatial stability of K_{2V} grains as better than 1–2 arc sec, but their sequence is only 4 min long.

Direct evidence that magnetic concentrations play a role in the K_{2V} grain phenomenon has been claimed by Sivaraman and Livingston (1982) from digital blink-comparison of Fe I 868.8 nm magnetograms and a series of K_{2V} spectroheliograms, taken sequentially with the Kitt Peak magnetograph (Livingston *et al.*, 1976). They report a one-to-one correlation between K_{2V} grains and magnetic elements, with all K_{2V} grains without exception corresponding to magnetic grains of 10–80 G. They also find that stronger K_{2V} grains correspond to larger field strengths, and that when magnetic features shift location between their two magnetograms, successive K_{2V} grains follow along. Sivaraman and Livingston state their case very definitely ('magnetism appears to be a necessary progenitor of the K_{2V} emission'); recently, Sivaraman (1991) has restated this claim.

However, we think it highly unlikely that K_{2V} cell grains correspond one-to-one with strong-field magnetic fluxtubes because we have found above that the occurrence of K_{2V} cell grains is fully determined by interference between two pervasive, ubiquitous oscillation patterns – leaving no room for another independent and intermittent grain localiser. How then to interpret the above observations?

We first note that Sivaraman and Livingston measured typical fluxes of only 10–20 G

for the magnetic elements which they equate to K_{2V} grains. Their magnetograms contain many more elements of similar flux. Such weak intranetwork flux concentrations cannot all be due to unresolved strong-field flux tubes, because recent observations with much higher spatial resolution display only a few strong-field elements in cell interiors (e.g., the magnetogram taken by Tarbell *et al.*, 1990, and shown in Figure 9 of Title *et al.*, 1990). Thus, only a few of the observed magnetic elements may correspond to strong-field flux tubes; most are, if significant, extended patches of weak field.

Secondly we note that while the magnetogram of Sivaraman and Livingston is full of such intranetwork elements, their K-line spectroheliogram is relatively empty in cell interiors. The spectroheliogram in their paper is the best in their series but its appearance differs strongly from Gillespie's spectroheliogram. It has only a few bright grains per cell, much less than the 10–20 seen on the latter. We attribute this discrepancy to differences in seeing and in passband. The 0.1 nm bandwidth of Sivaraman and Livingston equals the spectral bandwidth used by Cram and Damé for their H-index diagram. This diagram contains only the stronger K_{2V} grains; additional smearing by worse seeing reduces grain visibility yet further.

We are so led to suspect that the observed grains were not regular K_{2V} grains but correspond rather to the isolated strong-field features seen on Tarbell's magnetograms at similar spatial density. On K-line heliograms these should live longer than K_{2V} grains, show modulation primarily at 300 s periodicity and follow the migration to the nearest network boundary reported for intranetwork field elements by Martin (1990). We similarly suspect that such isolated 'magnetic grains' explain the long location memories reported by Damé (1985a). He used a passband with 0.12 nm FWHM, appreciably wider than the (full) 0.1 nm bandwidth of the H-index diagram, too wide to show regular K_{2V} grains properly.

2.2. Fourier domain

We now turn to the observational signatures of K_{2V} cell grains in the Fourier domain. There is so much variation in the diagrams of Cram and Damé that single-event descriptions such as those of Liu (1974) are to be taken with caution; they do not provide statistics, separation of frequency contributions or quantification of coherence and phase relationships. The oscillatory nature of the K_{2V} grains, of the K_3 Doppler manoeuvers, of the propagating whiskers and of the dark K_3 clouds discussed above clearly invites Fourier analysis in both the temporal and spatial domains.

Fourier papers of interest here are the pioneering analyses by the Meudon group, mostly of the Ca II infrared lines (Mein, 1966, 1971, 1978; Mein and Mein, 1976; Schmieder, 1976, 1977, 1978; Provost and Mein, 1979), the HIRKHAD analysis of Cram (1978), the phase studies of Lites and Chipman (1979) and Lites, Chipman, and White (1982), the K-line filtergram transforms of Damé, Gouttebroze, and Malherbe (1984) and Damé and Martić (1987), the CN analysis of Kneer, Newkirk, and von Uexküll (1982), the Hα oscillation studies of Kneer and von Uexküll (1983), 1985, 1986) and von Uexküll *et al.* (1989), and the Ca II infrared-line series by Deubner and Fleck (Deubner and Fleck, 1989, 1990; Fleck and Deubner, 1989).

The major paper addressing K-line Fourier behavior is the one by Cram (1978) who analyzed the HIRKHAD spectrogram sequence of Cram, Brown, and Beckers (1977). Cram assumed rotational symmetry on the solar surface to convert the one-dimensional HIRKHAD data (spatial resolution only along the spectrograph slit) with a modified Fourier transform into two-dimensional (k, ω) spectra showing power for the shifts and intensities of Ni I 589.3 nm, Na I D_2, Ca II 854.2 nm, Hα and the K_1, K_{2V}, K_{2R} and K_3 features of the K line core, and also for the intensity at $\Delta\lambda = 0.3$ nm and $\Delta\lambda = 0.09$ nm in the K line wing. In addition, he supplies (k, ω) diagrams of the coherency and phase differences between various pairs of these diagnostics.

Cram's (k, ω) diagrams add valuable information to the inventory of H and K cell grain properties. However, they mix the contributions from network boundaries and from cell interiors together, and the HIRKHAD sequence from which they have been measured has a duration of only 30 min. It is, therefore, of interest to compare them with the recent results of Deubner and Fleck (1990) who separated spectrograms containing Ca II 854.2 nm, Ca II 849.8 nm, and Fe I 849.6 nm (Fleck and Deubner, 1989) into contributions from cell boundaries and cell interiors. They averaged these contributions spatially, producing ω spectra rather than (k, ω) diagrams, and their sequence is much longer (4.5 hours); their results therefore have better statistics, temporal resolution and signal-to-noise than Cram's (k, ω) diagrams. The latter suffer much from the short duration, small spatial extent, one-dimensionality and poor statistics of the HIRKHAD series; nevertheless, they remain the only (k, ω) diagrams in the literature which permit comparisons between the velocity and intensity behavior of various Ca II K features with other lines.

2.2.1. *Response Heights*

The Fourier spectra in Figure 1 of Cram (1978) are arranged from top to bottom with increasing formation height (estimated heights of formation for the different lines are shown in Figure 1 of Cram, Brown, and Beckers, 1977). The line shift spectra (left-hand column) contain a well-defined area of enhanced power between 3 Mm and 20 Mm wavelength. It is confined to the 5-min regime for the weakest line (Ni I 589.3 nm) but shifts gradually towards shorter periods for lines of higher formation, extending up to 3 min for Hα and to 1.5 min for K_3. This shift towards higher frequency for increasing height of formation is well-known (Evans, Michard, and Servajean, 1963; Noyes and Leighton, 1963; Orrall, 1966; Frazier, 1968); a classic demonstration was given by Figure 1 (p. 299) of Noyes (1967). The upper-atmospheric 3-min 'high-frequency tail' has also been detected at longer wavelengths, in power spectra of molecular lines (Noyes and Hall, 1972; Deming *et al.*, 1986), of unresolved lines near 2.2 μm (Leifsen and Maltby, 1990), of the enigmatic Mg I 12 μm lines (Deming *et al.*, 1988), of submillimeter continua at 350 μm and 800 μm (Lindsey and Roellig, 1987), of the 3 mm continuum (Simon and Shimabukuro, 1971) and of the 3.3 cm continuum (Yudin, 1968).

Cram's intensity power spectra (second column in his Figure 1) show a similar drift of the high-power area towards shorter periodicity for Ni I, Na I D_2, and Ca II 854.2 nm, but this migration lags behind the drift in the line-shift diagrams in the first column. For

example, Na I D intensity behaves as Ni I shift and Ca II 854.2 nm intensity behaves as Na I D shift. This lag in power migration to shorter periods is a direct demonstration of the fact that velocity response heights can differ appreciably from intensity formation heights, an issue which we briefly discuss here because it affects the interpretation of observed phase differences between velocity and intensity fluctuations of one spectral line ($V - I$) and between the velocity fluctuations of two different lines ($V - V$).

Doppler shifts encode the emergent profile with the velocity field near optical depth unity, whereas the intensity response extends over a larger range, down to the layer where the *effective* optical depth reaches unity. For strongly scattering lines the geometrical difference between these two optical depths can be large. For example, the velocity response function for the Mg II k_3 core computed by Gouttebroze and Leibacher (1980) consists of a narrow peak near 2000 km height while the 'origin function' of this line, which describes the thermal creation of photons that eventually escape after many scatterings, peaks near 1000 km height and extends over the whole chromosphere. Similarly, the Ca II K_3 core originates from the top of the chromosphere in standard models (cf. Vernazza, Avrett, and Loeser, 1981) but its intensity responds sensitively to line source function fluctuations at the bottom of the chromosphere (e.g., Uitenbroek, 1989b). The case is even worse for Hα which has a doubly peaked contribution function (e.g., Schoolman, 1972).

Additional complications exist in the response of the Ca II lines to perturbations because H and K are influenced by the three subordinate Ca II infrared lines and vice-versa (Shine and Linsky, 1972, 1974; Uitenbroek, 1989b). These Ca II response effects have been computed in detail by Mein and his Meudon coworkers, unfortunately without much exposition. Mein introduced 'weighting functions', 'phase formation altitudes', 'transfer functions', and 'characteristic spatial wavelengths' (Mein, 1964, 1966, 1971). The weighting functions became known later as 'response functions' (Beckers and Milkey, 1975; Canfield, 1976; Caccin *et al.*, 1977; see also Magain, 1986). The phase formation altitudes describe average response heights to a passing wave in the limit of zero vertical wavenumber, while the transfer functions measure power gain and the characteristic wavelength divides the effects of waves into macroturbulent and microturbulent domains. Similar quantities were computed later by Mein and Mein (1976, 1980) and by Provost and Mein (1979).

A conclusion from these papers which is pertinent here is that the response of the weakest of the three calcium infrared lines, Ca II 849.8 nm, does not adhere to the naïve expectation that weaker lines display effects from deeper layers. Figure 3 of Mein (1971) and Figures 2–3 of Mein and Mein (1980) show that the intensity formation heights of Ca II 849.8 nm and Ca II 854.2 nm are similar, although their gf-value ratio is 9. These two lines have equal source functions because they share the same upper level; the population of that level is set by the K line so that the two infrared lines are strongly coupled to the K line. Their intensities respond, therefore, to perturbations at about the same height in the atmosphere (Shine and Linsky, 1974; Uitenbroek, 1989a). The velocity response of the weaker Ca II 849.8 nm line also peaks at this height (Mein, 1971; Mein and Mein, 1980), contrary to expectation.

These Ca II line formation intricacies may contribute to various inconsistencies between the Ca II 854.2 nm and 849.8 nm results of Deubner and Fleck (1990) and also to their disagreement with the earlier Ca II 849.8 nm results of Lites, Chipman, and White (1982). Clarification through detailed line formation modeling of the close coupling between this line and the K line is required, including effects of coupled partial frequency redistribution (cf. Rutten, 1990b).

2.2.2. *Lower Atmosphere*

The power spectra in Figure 1 of Cram (1978) exhibit a marked difference between the behavior of the deeper-formed diagnostics up to Ca II 854.2 nm (the top three diagrams in the first and second column) and the behavior higher up in the atmosphere (Hα and Ca II K Doppler shift and intensity). In this section we discuss the first group. Their power spectra show a well-defined high-power region which is centered at about 8 Mm spatial wavelength in all spectra and migrates upwards in temporal frequency for larger heights of formation, with the lag between line shift and intensity discussed above. The $V - I$ coherency and phase spectra (third and fourth columns) confirm the pattern: up to Ca II 854.2 nm the oscillatory nature is clearly established, with high coherence between shift and intensity and with maximum redshift leading maximum intensity by about 100°.

These atmospheric levels are also sampled by the extended wings of the K line for which Cram provides (k, ω) spectra in his Figures 3–5. The intensity power spectrum at $\Delta\lambda$ = 0.3 nm from K line center shows 5-min power but no 3-min power, just as the Ni I 589.3 nm line shift and intensity power spectra. This demonstrates that the K wing intensity provides a similar encoder as the Doppler shift of a normal Fraunhofer line, in agreement with the helioseismological South Pole measurements by Harvey and coworkers who obtain beautiful p-mode ridges in (k, ω) diagrams from broad-band K-line photometry (e.g., Jefferies *et al.*, 1988).

Closer to line center, the K wings possess more and more high-frequency power in their brightness fluctuations. The intensity power at 0.09 nm closely resembles the Na I D_2 intensity power spectrum, while the K_1 intensity power spectrum (Cram's Figure 4) resembles the Ca II 854.2 nm intensity power spectrum. Thus, these spectral features describe the same atmospheric layers. It follows that the oscillatory phenomena which cause the H and K wing whisker patterns discussed in Section 2.1 must also contribute to cell-interior power, phase and coherency spectra of lines up to Ca II 854.2 nm.

At the low frequency end, Cram's K-wing intensity power spectra contain power at about 10-min period and 4–9 Mm wavelength, which is the regime of gravity waves. Similar low-frequency power is also seen in the K_{1V}, K_{2V}, and K_{2R} intensity diagrams (Cram's Figure 5). This domain of the (k, ω) diagram is very sensitive to telescope guiding errors and the 30-min HIRKHAD sequence was too short to obtain good statistics; nevertheless, Cram thought the power significant because the coherence between the two K-wing intensities at 0.3 and 0.09 nm from line center is very high. Their phase difference is negative, implying downward phase velocity which corresponds to

upward energy transport. Cram suggested that this power signifies the existence of gravity waves that are presumably excited by granules or other convective elements. They had been noted earlier by Schmieder (1976); a beautiful confirmation is given by the $V - V$ phase surface of Deubner and Fleck (1989) where they indeed occupy the same (k, ω) location.

At higher frequencies, Fleck and Deubner (1989) and Deubner and Fleck (1990) add much temporal Fourier information to Cram's spectra. They confirm once more that the 3-min power arises primarily from cell interiors and that cell boundaries oscillate more strongly at 5-min periodicity. The regime of evanescent waves, at 3–5 min periodicity, displays downward traveling phase in the Ca II 854.2–849.8 nm V–V diagram for cell interiors, which is puzzling. In the acoustic regime (periodicity below 3 min) the $V - V$ phase travels upward and increases with frequency but stays small, much smaller than one would expect for running acoustic waves. This behavior is also displayed by Cram's phase and coherency (k, ω) diagrams, although less clearly. For example, his $V - V$ diagram for the Na I D_2 – Ca II 854.2 nm pair shows a slow increase of phase difference with frequency in the acoustic regime; a similar increase is present in the Ni I 589.3 nm – Na I D_1 $V - V$ phase diagram. Fleck and Deubner (1989) take the smallness of the $V - V$ phase increase to imply 'the existence of a standing wave pattern for the whole continuum of acoustic waves with frequencies beyond the acoustic cut-off frequency', as was done before by Mein and Mein (1976) and Provost and Mein (1979), who invoke magneto-acoustic wave reflection on the steep temperature increase in the chromosphere-corona transition region. However, there are no 180° phase jumps which standing waves should produce at the frequencies for which the velocity response height coincides with a nodal plane (Provost and Mein, 1979); their absence leads Fleck and Deubner (1989) to infer that something drastic happens near the 'magic height' of 800–1200 km.

Additional puzzles are posed by the phase shifts between velocity and brightness about which Deubner (1990) has recently summarized various observations. His Figure 1 confirms Cram's display of $V - I$ phase difference of about 100° up to Ca II 854.2 nm, displaying phase shifts of about this value throughout the 2–5 min regime. (Note that 100° in Cram's definition of $V - I$ which we follow here – redshift leading brightness – translates to 80° in Deubner's $I - V$ figures.) There is a steep transition at 2.2 mHz (7.5 min) towards large $V - I$ phase difference at lower frequencies for all deeper-formed lines. It was observed earlier by Lites and Chipman (1979) and it may have to do with the 'missing piece of phase cake' of Marmolino and Severino (1990) and the unexpected ridge-to-interridge phase jumps shown in Figure 2 of Deubner (1990). These have recently been discussed in more detail by Deubner *et al.* (1990). However, these phenomena are probably not important within our context of the Ca II cell grains since the latter originate in higher layers and higher up in the (k, ω) diagram.

In his Figure 3, Deubner (1990) has plotted the 5-min and 3-min phase behavior against height of formation. The steep transition is here seen to occur below 300 km; above that height, the $V - I$ phase lag smoothly increases from about 60° to about 100°

at the Ca II 854.2 nm velocity response height. This behavior extends to high frequencies (2-min periodicity) in Figure 6 of Deubner and Fleck (1990), with high coherency for the cell interior. Independent evidence for this outward increase in $V - I$ phase comes from the recent observations of oscillations of the infrared CO lines by Ayres and Brault (1990). They observe $V - I$ lags of 70° for the stronger CO lines and of 40° for the weaker ones. Further evidence is supplied by the infrared continuum data of Lindsey and Roellig (1987) who observe about 30° phase delay between brightness fluctuations in the 350 μm and 800 μm continua. As pointed out by Deubner (1990), $I - I$ phase differences between intensities formed at different heights reflect the change with height of $V - I$ phase differences found from single lines for which V and I respond to about the same height. The reason is that the change in $V - V$ with height for line pairs formed at different altitudes is negligible, the $V - V$ shifts being small anyhow. The infrared $I - I$ phase lag indeed fits well in Deubner's $I - V$ diagram.

The $I - I$ phase differences of the outer wing of the K line display similar behavior. Cram's $I - I$ diagram for the $\Delta\lambda = 0.3$ nm and $\Delta\lambda = 0.09$ nm pair (his Figure 3) shows lags of 10–30° in the 3–5 min regime, in agreement with Deubner's $I - V$ diagram. However, Cram's $I - I$ phase diagram for the $\Delta\lambda = 0.3$ nm and K_{1V} pair (his Figure 5, top left) which covers a larger interval in formation height, displays a distinct pattern of $I - I$ phase lag increase with temporal frequency, from 30° at 5 min to 90° at 2 min which exceeds the $I - V$ differential behavior in Deubner's figure. Compatible behavior is seen in Cram's $V - I$ diagram for Fe I 393.3 nm velocity and $\Delta\lambda = 0.3$ nm intensity (his Figure 5, top right). This diagram shows decreasing $V - I$ phase lag with temporal frequency, from about 120° at 5 min to 0° at 2-min periodicity. In this case, the V signal is formed at higher altitude than the I signal; the latter signal therefore precedes the phase of the intensity at the height where V is formed for 2-min periodicity by just the amount of the local $V - I$ lag.

How do these findings correspond to the spatio-temporal K-wing behavior which we discussed in Section 2.1? The $V - I$ quarter-wave phase lag (maximum redshift leading maximum brightness) in the Fourier diagrams confirms the pattern in the event descriptions of Liu (1974), Beckers and Artzner (1974) and Cram, Brown, and Beckers (1977) in which redshifts generally precede brightenings; the Fourier diagrams quantify this pattern by virtue of better statistics. Thus, the power, phase and coherency spectra of the K wing and of lines up to Ca II 854.2 nm indeed provide another view of the H and K wing whisker patterns. Similarly, the quarter-period $V - I$ phase difference for the inner wing oscillations of Hα measured by Giovanelli (1975) indicates that this diagnostic also addresses the phenomenon which causes H and K whiskers.

Cram's $I - I$ phase shifts translate directly into the observed whisker contractions in the wings of H and K. For 3-min periodicity, the 30° phase lag between $\Delta\lambda = 0.3$ nm intensity and $\Delta\lambda = 0.09$ nm intensity (Cram's Figure 3) corresponds to a time lag of 15 s in the spectrum or a whisker contraction speed of 0.014 nm s^{-1}, in good agreement with the whisker observations of Liu (1974) and Beckers and Artzner (1974). Closer to the core, the phase difference between $\Delta\lambda = 0.09$ nm intensity and K_{1V} intensity is also about 30° for 3-min periodicity, corresponding to about 7 pm s^{-1}. This is faster than

the contraction of the inner triangular parts of the whiskers seen in the time-resolved spectra of Cram and Damé, which is about 1 pm s^{-1}. The higher the frequency, the larger the $I - I$ phase lag in Cram's Figure 5 and the slower the corresponding whisker contraction; this suggests that the observed whisker slow-down near line center follows from increasing contribution by high-frequency components.

2.2.3. *Upper Atmosphere*

For the higher-formed K-line features of Cram (1978) there are no corresponding data from Deubner and Fleck, but there is comparison material in the Hα Fourier studies of Kneer and Von Uexküll. Cram's Figure 1 demonstrates clearly that something drastic happens when going from Ca II 854.2 nm to Hα and K_3: *the intensity power behavior drops out of the pattern set by the weaker lines.* The velocity power spectra continue the trend set by the lower-formed diagnostics, with K_3 reaching up to about 2-min periodicity, good coherence between Hα and K_3 shifts for small wave numbers (Cram's Figure 2) and with small $V - V$ phase differences (Cram's Figure 2), but the patch of high power present in the line shift spectra vanishes abruptly from the intensity power spectra. They are nearly devoid of power in the 3-min region. K_3 shows some power at small wave numbers in the 5-min region but Hα does not.

These diagrams confirm the picture that we gleaned above from Cram and Damé's space-time diagrams. At the K_3 level there is a pervasive Doppler oscillation which reaches high temporal frequencies, differs from the oscillation in deeper layers, does not possess much brightness modulation and is best seen in the V/R space-time diagram. Indeed, in the Fourier spectra K_3, shift behavior is most closely reflected by K_{2V} intensity: the K_{2V} intensity power spectrum is the only one which resembles the K_3 line shift power spectrum. In contrast, the $K_{2R}(k, \omega)$ diagram is nearly devoid of power.

Cram finds high coherence between K_3 shift and K_{2V} intensity for 2–5 min periodicity and wavelengths above 6 Mm, with small phase difference. He also finds rather high coherence in the same region between Na I D_2 redshift and K_{2V} intensity, with about 120° phase difference just as for the shift and intensity of Na I D_2 itself. The latter fit in the lower-atmosphere oscillation pattern. Thus, K_{2V} intensity behavior depends both on the K_3 shift and on the whisker modulation, i.e., on a mixture of the two types of oscillation. This confirms our conclusion from the space-time diagrams that the appearance of cell grains is set by interference between these two distinct oscillation patterns.

Additional Ca II power spectrum analysis has been supplied by Damé, Gouttebroze, and Malherbe (1984) from their K-line filtergram sequence. The large width of their passband (0.12 nm FWHM) implies that their intensity signal primarily depicts the whisker intensity modulation, with some K_3 Doppler influence on the K_{2V} intensity. Their (k, ω) diagram agrees roughly with Cram's K_3 intensity power spectrum; they claim to see detailed ridge structure which we deem unconvincing. They also claim significant power in the gravity wave domain, with wavelengths above 3 Mm and periodicities above 10 min. This agrees with Cram's finding of power in the same (k, ω) domain in his K-wing (k, ω) diagrams; in fact, his K_3 diagrams also show some indication of extra power at low frequencies and small wave numbers. This finding of

gravity-wave power for K_3 implies that these waves, if they exist, persist to large height.

Let us now turn to Hα. Cram's line shift power spectra indicate that the Hα shift originates deeper than the K_3 shift. His $V - V$ diagrams for the two lines show high coherency up to high temporal frequency, corresponding to 80 s periodicity, with negligible phase lag for spatial wavelengths above 5 Mm. Thus, the K_3 Doppler oscillation also affects Hα line center. This is confirmed by the observations of von Uexküll *et al.* (1989) whose Figure 3 displays temporal power spectra for Hα line-center shift and brightness fluctuations, separated into cell interior and cell boundary contributions. As for K_3, there is much power in the 2–5-min region for the shift but almost none for brightness. The $V - I$ phase difference is again 90°, except for high frequencies (periodicities below 100 s) for which the lags reach 180°.

A final point to make is that the area of enhanced power occupies nearly the same wavenumber range in all of Cram's (k, ω) diagrams, typically from 3 Mm to 20 Mm wavelength and centered on about 8 Mm wavelength. In the higher layers this average wavelength equals the value derived later by Damé and coworkers from K filtergrams and TRC 160 nm filtergrams. Apparently, all oscillatory patterns that we have discussed have 8 Mm as characteristic wavelength. This is also the scale of the mesogranular horizontal flow pattern (November *et al.*, 1981), the scale on which 'active granules' appear to be organised (Oda, 1984) and the scale of the long-duration brightness patterns observed in the Mg I b_2 line by November (1989). This scale equality has led Damé and Martić (1987) to write of 'chromospheric mesogranulation' for the K-line oscillations and to speak of a direct connection between these convective and oscillatory mesoscales (p. 252 of Rutten and Severino, 1989). The issue has been addressed by Deubner (1989a, b). He concludes that the photospheric mesogranular pattern is a truly convective phenomenon, but leaves the question open whether there is a direct relation between mesogranulation and the spatial properties of the oscillations in the higher atmosphere.

3. Models and Simulations

In this section we review modeling efforts concerning K_{2V} cell grains. We also add computations of our own to illustrate various possibilities. Our objective for the latter is not to produce a consistent model of K_{2V} grain evolution here – that requires extensive numerical simulation – but to demonstrate how existing models fail.

We divide K_{2V} grain models into two classes. The first class consists of *ad hoc* temperature and velocity perturbations which are applied to a static model atmosphere. Such models serve to investigate the effect of macroscopic velocity fields on computed line profiles, the arbitrary choice of velocity field providing full freedom to experiment and study line profile response. The second class consists of numerical simulations in which the response of the atmosphere to pressure and temperature disturbances is computed time-dependently and self-consistently from the hydrodynamics equations.

3.1. AD HOC MODELS

The first K_{2V} model in the literature is the one by Jewell (1900) who lets meteorites collide with updrafts: "The bright emission components (of H and K) may possibly be caused by the downrush of this meteoritic matter through the denser portions of the chromosphere such that where it meets the uprush of the (ascending) matter, the impact of the collisions or the friction caused produces an intense emission of certain lines in this region of the chromosphere." StJohn (1910) was the first to interpret the redshift and asymmetry of H and K as due to mass motions within the solar atmosphere. Since then, the K_{2V} phenomenon has often been attributed to macroscopic velocities (e.g., Miyamoto, 1958; Suemoto, 1963; Athay, 1970; Cram, 1972a, b, 1974; Liu and Skumanich, 1974; Grossmann-Doerth, Kneer, and von Uexküll, 1974; Durrant, Grossmann-Doerth, and Kneer, 1976; Mein *et al.*, 1987).

There are two basic possibilities to generate the observed asymmetry with bright K_{2V} emission but no K_{2R} emission from velocities: upward motion of the K_2 layer or downward motion of the K_3 layer (e.g., Athay, 1970; cf. Hummer and Rybicki, 1968). The data show that grains and large K_3 redshift come together; inspection of the tracings in Figure 2 of Damé (1984) suggests that the H_3 redshifts reach up to 10 km s^{-1}. Mein *et al.* (1987) have evaluated these shifts using a series of H-line profiles from the Cram and Damé spectra. They use a sophisticated technique in which observed profiles are fitted by automatic adjustment in a nonlinear, Fourier perturbation scheme, resulting in the inversion of the observed time-dependent profile into consistent sets of four parameter values: the size and the slope of temperature and velocity perturbations to a standard model atmosphere, with linear height dependence. Their results demonstrate that H_{2V} events are produced by large downward velocity gradients associated with temperature enhancements, with large downward velocities at H_3 forming heights, 5–10 km s^{-1}, in agreement with the values measured directly from the spectra without radiative transfer interpretation.

K-line profiles have been computed with the assumption of such large K_3 redshifts by Athay (1970), Cram (1972a), and Liu and Skumanich (1974). These confirm that the H and K profile shape at the moment of the K_{2V} flash can be reproduced with large K_3 downflow. For example, Liu and Skumanich (1974) fitted a K_{2V} grain observed by Liu (1974) with an atmosphere to which they applied an upwards moving temperature perturbation and a 10 km s^{-1} downdraft at the K_3 formation level, with rapid decrease of speed with depth below this level. Their *ad hoc* model reproduces the bright wing whisker prior to the K_{2V} bright point from the temperature disturbance and the K_{2V} flash from the redshift of the core. They do not fit other stages of the K_{2V} phenomenon, such as the fast blueward recursion of K_3 after the grain, or the observed absence of K_{2R} grains. These other stages are also not reproduced by *ad hoc* models employing sinusoidal wave representations. If these produce a proper K_{2V} peak in the part of a cycle when the K_3 layer moves down, they also produce a K_{2R} peak of similar strength and behavior when the K_3 layer moves up (e.g., Shine and Oster, 1973; Section IVb of Scharmer, 1984).

3.2. WAVE AND SHOCK SIMULATIONS

In *ab initio* simulations the fluctuations in velocity, temperature, pressure, and density are in principle computed self consistently from the hydrodynamics equations and not chosen arbitrarily to match observed profiles. However, there is still freedom in the choice of boundary and initial conditions and the problems of radiative cooling (and heating) are sufficiently large that considerable simplifications are necessary. Examples are the wave and shock computations of Stein and Schwartz (1972), Heasley (1975), Cram (1976), Ulmschneider *et al.* (1977), Kalkofen and Ulmschneider (1977), Hammer and Ulmschneider (1978), Gouttebroze and Leibacher (1980), Leibacher, Gouttebroze, and Stein (1982), Ulmschneider (1986), and Gouttebroze (1989).

Some of these analyses describe the effects on K-line profiles of a single acoustic pulse that travels upward through an initially motionless atmosphere, accounting for local temperature and density variations and shock formation. The result is an asymmetric profile with enhanced K_{2V} emission but without K_3 shift when the pulse arrives in the K_2 layer, and enhanced K_{2R} emission with a shift of K_3 to the blue when the pulse passes through the K_3 forming layer. Such single pulse models do not explain the observed gradual excursion of K_3 towards the red. Figure 3 of Cram (1976) gives an example. The K_3 core stays in place while the K_{2V} peak grows in intensity. A smaller emission peak develops at K_{2R} at the same time, the asymmetry being due to the blueshift of the K_2 layer. The pulse then reaches the K_3 layer; the core blueshifts in agreement with the observations, but it also produces further brightening of the K_{2R} peak which is only rarely observed.

Similar results were obtained by Gouttebroze and Leibacher (1980) who computed profiles of the Ca II H and K and Mg II h and k lines for an acoustic pulse in their experiment (a). They solved the full nonlinear one-dimensional hydrodynamics equations and treated the line formation with partial redistribution. Their profiles (their Figure 2(b)) have large K_{2V} and K_{2R} peaks already in the undisturbed atmosphere; the two peaks wax and wane in alternation during the passage of the pulse. In contrast, the darkest decile of the observed H-line profiles of Cram and Damé (1983) has no H_2 peaks, only a tiny bulge at H_{2V}; there is no H_2 emission at all in the darkest profiles in Figure 2 of Damé (1984).

Gouttebroze and Leibacher (1980) also performed numerical experiments in which they excited the atmosphere at its bottom with a train of pressure perturbations of 300 s periodicity, and then let it oscillate freely thereafter. The resulting oscillations of the upper atmosphere show quasi-periodicity of 200 s, with 90° phase retardation between temperature and velocity. Similar oscillations are present as a 'wake' at the acoustic cut-off period in Figure 10 of Stein and Schwartz (1972); their persistence was ascribed by Leibacher, Gouttebroze, and Stein (1982) to standing-wave resonance of a chromospheric cavity bounded by the transition region at its top, suggested earlier by Mein and Mein (1976) and Provost and Mein (1979). Leibacher, Gouttebroze, and Stein argue that these 200 s oscillations are present throughout the atmosphere, but decay less rapidly with height than the 300 s oscillations because they are much closer to the

acoustic cut-off frequency and therefore gain domination above 1000 km. Their waveforms steepen from sinusoidal to sawtooth shape above 1700 km. A sequence of Ca II K-line profiles from this simulation is shown in Figure 7 of Gouttebroze and Leibacher (1980). The profile changes are remarkably similar to the single-pulse results of Cram (1976), the only difference being that K_3 now Doppler shifts both to the red and to the blue during the cycle. There is still symmmetry in this Doppler behavior: a K_{2R} peak develops while K_{2V} reaches maximum brightening and an equally intense K_{2R} peak appears afterwards. Compared to the observations, the whole pattern is yet too sinusoidally symmetrical. Also, there is no phase without K_2 emission features.

3.3. Numerical illustrations

In this section we present three sets of computations which illustrate various modeling options. In the first set an *ad hoc* velocity disturbance of shock-like dimension is applied to a standard atmosphere. It demonstrates that sizable K_3 downdrafts are needed to reproduce the V/R asymmetry and K_3 Doppler behavior. The second set concerns wave perturbations of a cool model atmosphere; it serves to illustrate that simple acoustic wave models do not produce the observed standard evolution pattern. In the third set a train of periodic shock waves travels upwards through the atmosphere. It reproduces some aspects of K_{2V} evolution but yet fails to provide sufficient K_3 downflow.

3.3.1. *Atomic Model, Atmospheric Model and Method*

We compute K-line profiles from a five-level plus continuum representation for Ca II, including the $4s^2S^e$ ground level, the two metastable $3d^2D^e$ levels and the two $4p^2P^o$ levels. These five bound levels provide an adequate description of the formation of the K line in the solar atmosphere, provided all five radiative transitions between them (H, K, and the IR lines at 849.8 nm, 854.2 nm, and 866.2 nm) are included. We treat only the K line with partial redistribution, which is a suitable approximation when one is only interested in this line (cf. Uitenbroek, 1989b). As atmospheric model we use the A' one-dimensional atmosphere which is the coolest model of the standard Harvard grid (Vernazza, Avrett, and Loeser, 1981) as modified by Avrett (1985). In the shock wave experiments we also use a modified model with a less steep chromospheric temperature increase.

We solve the coupled equations of radiative transfer and statistical equilibrium with the iterative Newton–Raphson scheme described by Uitenbroek (1989b). This is an extension of the Scharmer and Carlsson (1985) method to the more general case of scattering with partial frequency redistribution. A difficulty arises concerning the redistribution over angle in the resonance scattering. Angle-averaged redistribution functions are valid for the K line in a static atmosphere without macroscopic velocity fields (Milkey, Shine, and Mihalas, 1975a), and they remain a reasonable approximation if the systematic velocities do not exceed the non-thermal broadening (cf. Mihalas and Kunasz, 1986). For larger velocities there are two possible solutions. The first is to use angle-dependent redistribution functions, with the disadvantage that the numbers of

frequencies and angles increase appreciably. The second is to solve the transfer equation in the co-moving frame. However, the transfer equation is then a diffusion-like partial differential equation with derivatives to both depth and frequency; it is difficult to specify the higher order boundary conditions one needs for strong lines such as the K line. Moreover, the numerical scheme of our code makes it difficult to use the co-moving frame method in atmospheres with non-monotonic velocity fields, because sign reversal decreases the stability of the frequency integration. We therefore use angle-averaged redistribution where possible and the co-moving frame formulation for large velocities, accepting that we can only treat monotonic velocity change in the latter case.

3.3.2. *Ad hoc Shock*

Our first example illustrates K_3 Doppler signature. It is similar to the t = 120 s moment of the model of Liu and Skumanich (1974) in assuming a large downward velocity in the K_3 forming layers combined with a steep velocity gradient below them. We step this *ad hoc* velocity pattern through the model atmosphere to mimic upward propagation; in contrast to Liu and Skumanich we do not perturb the temperature and density.

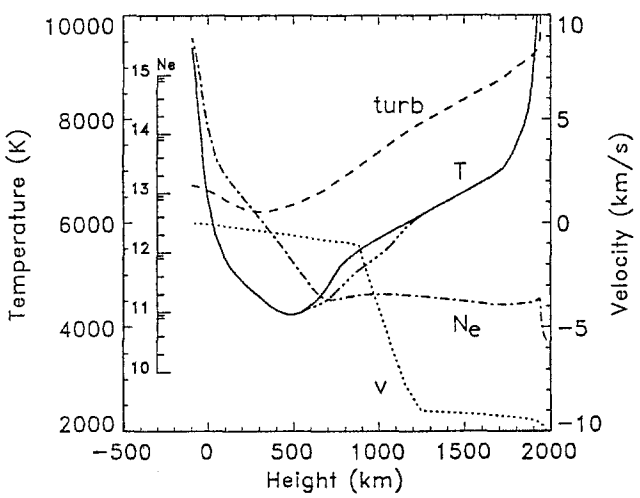

Fig. 3. *Ad hoc* shock front velocity (dotted) and stratification of temperature (solid), microturbulence (dashed) and log electron density (dot-dashed) of model A' of Avrett (1985). The modified temperature structure used in the shock train computation is also shown.

Figure 3 shows the adopted velocity structure together with the run of temperature, electron density and microturbulence of model A' and the temperature stratification of a modification of model A', which is used in our shock train illustration. The velocity profile has an 8 km s^{-1} step, with tails to provide monotonicity. Figure 4 shows resulting K-line profiles. The uppermost profile is for the undisturbed model A'; it equals the corresponding A' profile in Figure 18 of Avrett (1985).

It has symmetrical K_2 peaks, indicating that model A' is too hot in the low chromo-

sphere to reproduce the darkest H and K cores seen on the Sun. The other profiles result from stepping the velocity structure through the atmosphere. They possess two properties which are characteristic of observed K_{2V} cell grains. The first is the enhancement

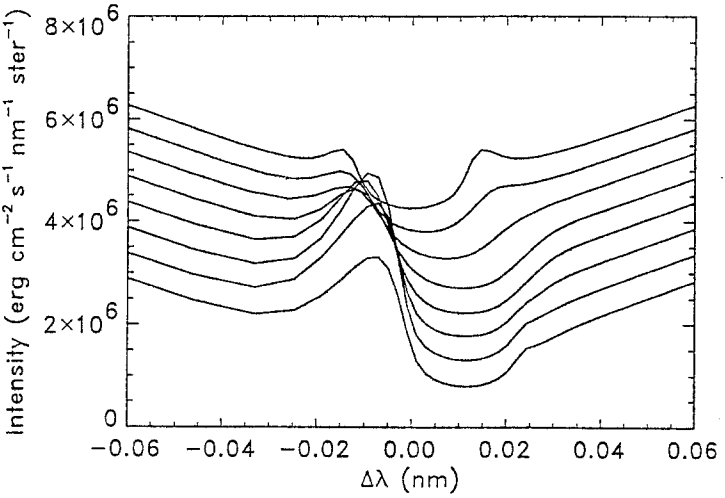

Fig. 4. K-line profiles for *ad hoc* shock travelling outwards through model *A'*. Each successive profile has been shifted upward by the same amount. Two full cycles are shown.

of the violet peak, which results from red-shifting the K_3 core, so that its opaque material obscures K_{2R} while unveiling K_{2V}. This is illustrated in Figure 5 which shows the Planck function at the wavelength of the K line together with the K-line source function for two different wavelengths, + 0.01 nm and − 0.01 nm from line center at rest. The arrows

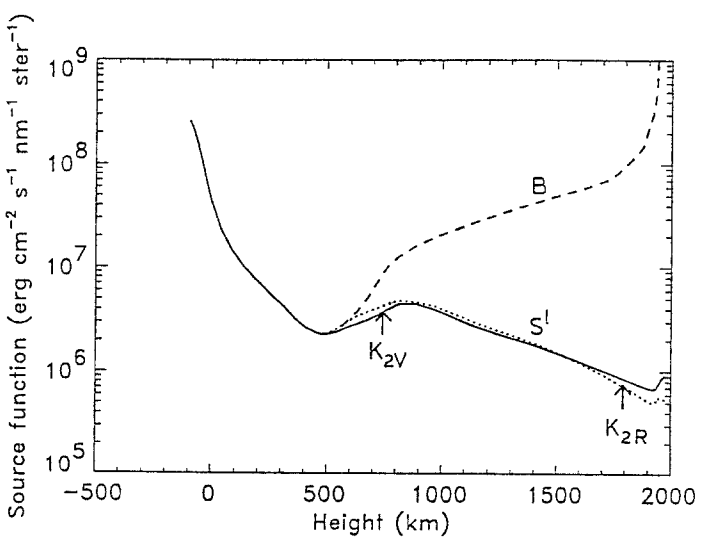

Fig. 5. Planck function at K-line wavelength (dashed) and line source functions for $\Delta\lambda = -0.01$ nm (solid) and $\Delta\lambda = +0.01$ nm (dotted) from line center. Arrows mark location of optical depth unity for $\Delta\lambda = -0.01$ nm (left) and $\Delta\lambda = +0.01$ nm (right).

mark the heights where the optical depth reaches unity at these wavelengths; at $\Delta\lambda = -0.01$ nm (left-hand arrow) this location samples the line source function at a deeper level, where it is more closely coupled to the chromospheric temperature rise, than for $\Delta\lambda = +0.01$ nm; the resulting K_{2V} peak is much higher than the K_{2R} peak. The second property is the quick recursion of the K_3 core to its rest position while the steep velocity gradient moves through and out the K_3 forming layer.

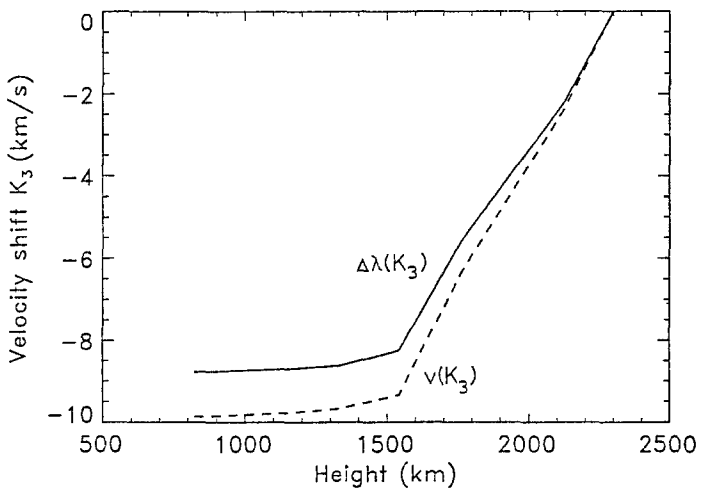

Fig. 6. Velocity shifts of profiles from the *ad hoc* shock model. Solid: velocity inferred from Doppler shift of K_3. Dashed: true velocity at height with optical depth unity for K_3. Abscissa refers to position of center of front in atmosphere.

Figure 6 shows the input velocity at the height where the K_3 optical depth reaches unity (dashed) as well as the Doppler velocity measured from the shift of the K_3 minimum. This comparison demonstrates that the observed K_3 Doppler shift provides a reliable measurement of the true velocity at the K_3 formation height, confirming the similar conclusion of Gouttebroze and Leibacher (1980) and the profile interpretation scheme of Mein *et al.* (1987).

3.3.3. *Acoustic Wave*

When waves or shock trains travel upwards through the atmosphere, downflows are followed by upflows. Models with a single cycle of equal up and down motion (e.g., Cram, 1976) produce a K_{2R} peak for every K_{2V} peak, one after the other, in conflict with the observed preponderance of K_{2V} peaks (Durrant, Grossmann-Doerth, and Kneer, 1976).

Cram, Brown, and Beckers (1977) have proposed a wave model that may suppress the concurrent K_{2R} emission. It consists of a vertical velocity field of the form:

$$v(z, t) = v_{\mathrm{ph}} \exp(z/H_v) \cos[2\pi(t/P - \phi(z))] , \tag{1}$$

where z is the geometrical height, v_{ph} the velocity amplitude in the photosphere, H_v the

velocity scale height due to the density stratification and $\phi(z)$ a depth-dependent phase function. Cram, Brown, and Beckers (1977) approximated the latter by the linear function $\phi(z) = z/L$ with $3 < L < 10$. The temperature perturbation lags behind the velocity perturbation in phase, in agreement with the observations, so that there is maximum heating in the K_2 forming layers when K_3 shows maximum redshift while half a period later, at the moment of maximum K_3 blueshift, the temperature reaches its minimum which may suppress the appearance of a red peak.

TABLE I

Formation heights (Mm) and phase lags (degrees)

Line	Height	Phase lag
Ni I 589.3	0.3	0
Na I D_2	0.9	60
Ca II 854.2	1.3	90
Hα	1.6	120

We have tested Equation (1) by generating K-line profiles, adopting 1.2 Mm for H_v and 1.0 km s^{-1} for v_{ph}. The phase lags $\phi(z)$ (for 200 s waves) are specified in Table I; they are from Cram (1978). The line formation heights are from Figure 2 in Cram, Brown, and Beckers (1977), with zero height defined at continuum optical depth unity at 500 nm. We compute appropriate temperature and density perturbations from the velocity $v(z, t)$ and the local sound speed (e.g., Mihalas and Mihalas, 1984, p. 172). Figure 7 shows the velocity v and the corresponding temperature perturbation ΔT with

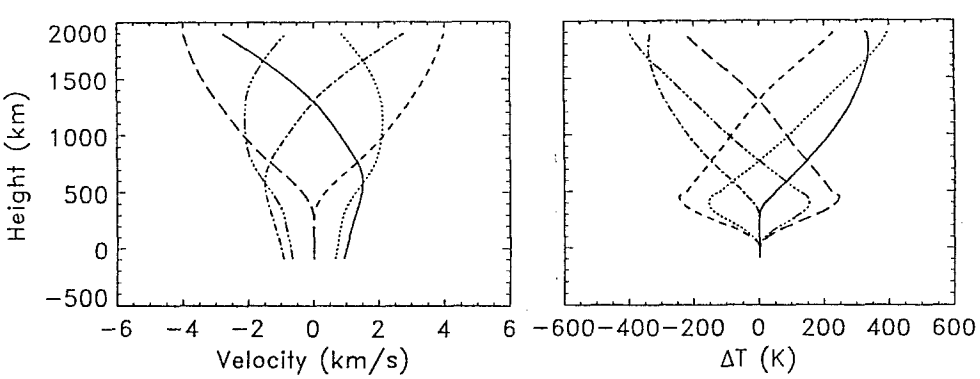

Fig. 7. Acoustic wave model. *Left*: velocity perturbations. *Right*: temperature perturbations. Coding: phases 0 ——, $\frac{1}{8}$ · · · ·, $\frac{1}{4}$ - - - -, $\frac{1}{2}$ – · – · –, $\frac{5}{8}$ – · · · –, and $\frac{3}{4}$ – – –.

height for six different phases; Figure 8 shows the emergent K-line profiles. Two cycles are shown to give a better impression of the changes. Starting with an unshifted 'dark' profile for phase 5/8*P* (see Figure 7), without K_2 emission peaks, the wings brighten because the temperature increases in the upper photosphere. K_3 shifts towards the red

and a K_{2V} emission peak appears. The K_3 reversal then shifts back again with the same spectral speed (due to the cosine in Equation (1)) and so produces a red emission peak, which is less pronounced than its violet counterpart because the temperature perturba-

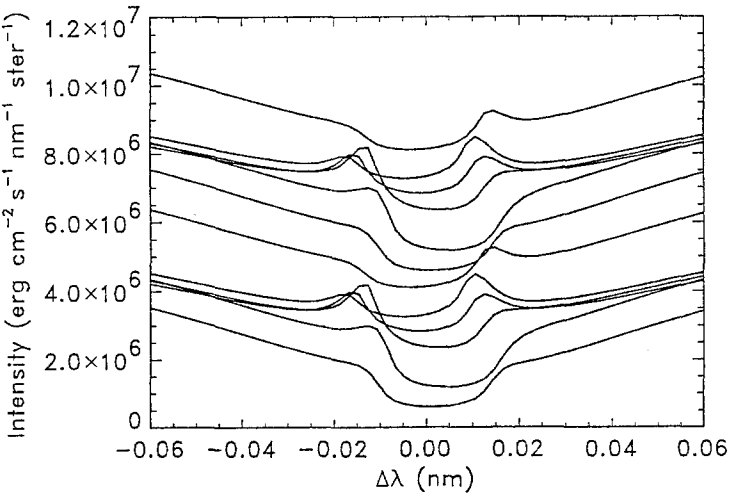

Fig. 8. K-line profiles for acoustic wave model. Two cycles have been plotted. Each profile has been shifted upwards by an amount proportional to the elapsed time.

tion is then negative (phases $1/2P$ and $1/4P$). The symmetry of the line shift pattern is also evident in Figure 9, which again shows excellent agreement between the specified velocity and the measured wavelength shift. This model does produce wing brightening and enhanced K_{2V} emission, but the parameter values used here do not give the observed sawtooth pattern and amplitude asymmetry of the K_3 shifts. There is also still too much K_{2R} emission.

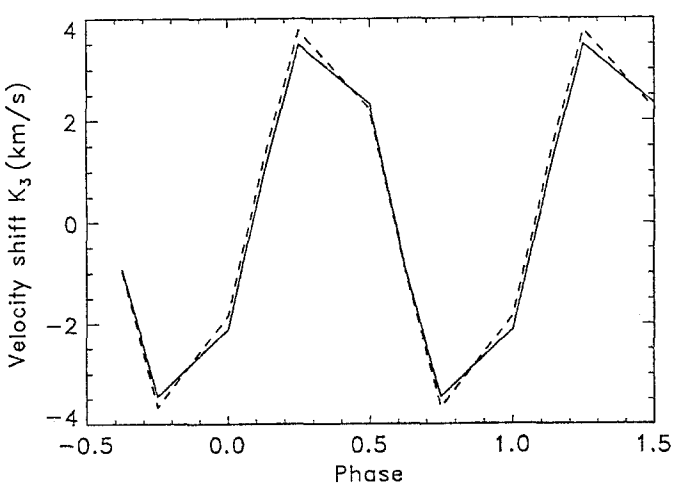

Fig. 9. Velocity shift of K_3 for acoustic wave model. Coding as in Figure 6.

3.3.4. *Shock Train*

The observed sawtooth Doppler shift pattern of K_3, with excursions of 5–10 km s^{-1}, is a direct indication of nonlinear behavior in the higher atmosphere and perhaps of the presence of shocks. The velocity of sound is about 7 km s^{-1} throughout the photosphere (Canfield and Beckers, 1976), so that the largest observed Doppler shifts correspond to material velocities exceeding the sound speed. The observed sawtooth asymmetry in which a slow K_3 shift towards the red is followed by rapid recursion to the blue after the wing brightening reaches line center suggests that the next disturbance travels upwards into the downflow of infalling matter from the previous one. Such behavior is seen above h = 1700 km in the simulations of Gouttebroze and Leibacher (1980) and Leibacher, Gouttebroze, and Stein (1982), in which 'waveforms change to a narrow overpressure, temperature, or density spike at the leading edge of the velocity sawtooth, with nearly constant ambient conditions through the remainder of the cycle. The narrow pressure pulse blasts the atmosphere upward, after which the atmosphere follows a ballistic trajectory until the following pulse reverses the motion'.

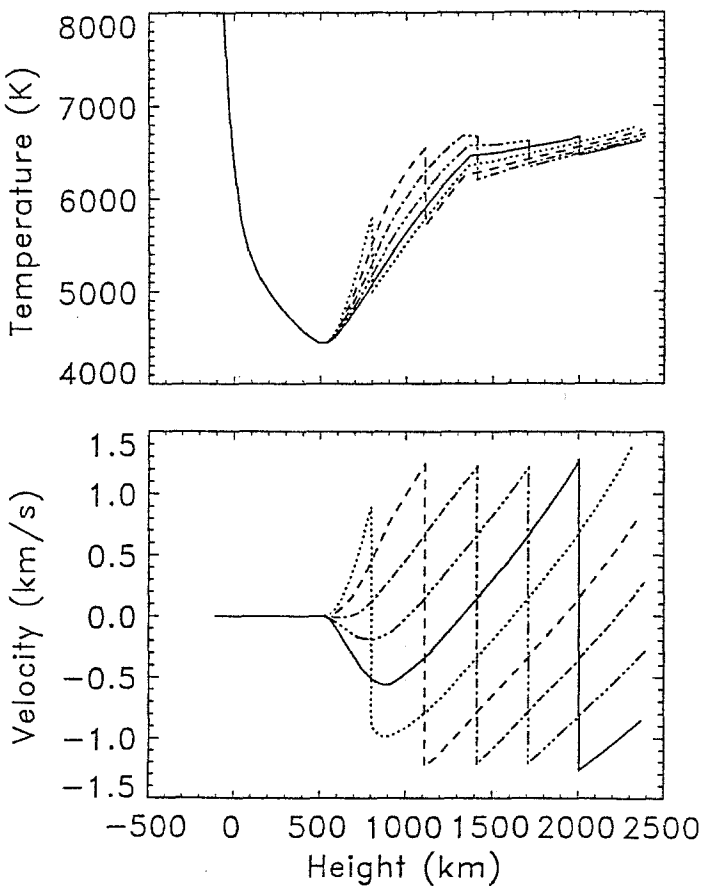

Fig. 10. Temperature (top) and velocity (bottom) stratifications of shocks for model A'. Shock strength Mach 1.2. Coding: phases 0 —, $\frac{1}{8}$ ····, $\frac{1}{4}$ – – –, $\frac{1}{2}$ –·–·–, $\frac{5}{8}$ –···–.

In these simulatons this behavior occurs too high to affect H and K line formation, as is clear from the sinusoidal behavior of K_3 in the results of Gouttebroze and Leibacher (1980), but similar shock trains, with ballistic downfall between successive shocks, may represent a viable explanation for the repetitive K_{2V} phenomenon if they occur deeper in the atmosphere. We test this option by computing K-line profiles from propagating shocks of arbitrary strength, using a program kindly provided by A. A. van Ballegooijen. We perturb a model atmosphere above 500 km height with a sequence of upward propagating shocks with 200 s periodicity (Figure 10). The dynamical behavior of the plasma is approximated by assuming constant acceleration of the gas

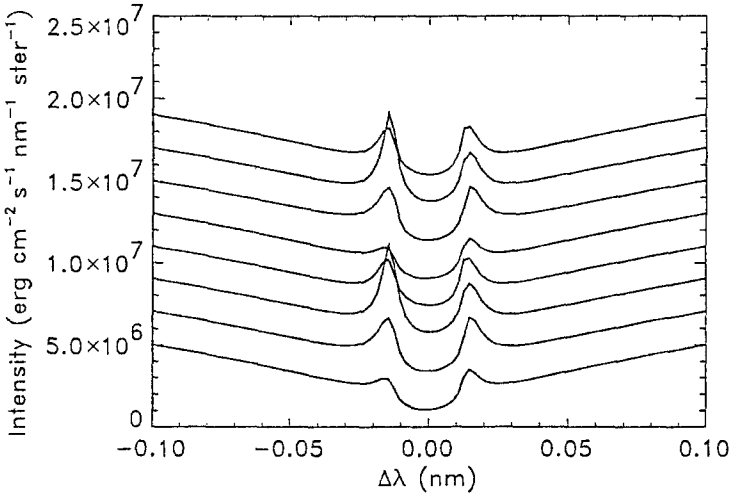

Fig. 11. K-line profiles of a series of shocks of Mach 1.2 for model A'. Each successive profile has been shifted upwards by the same amount. The intensity scale is for the bottom profile. Two full cycles are shown.

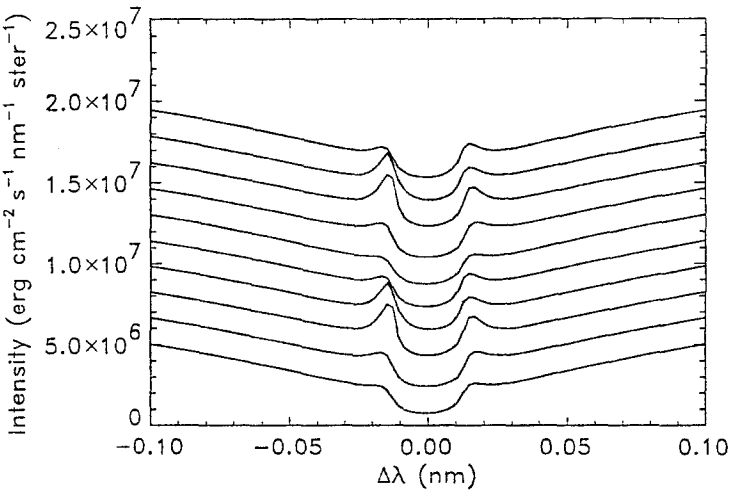

Fig. 12. K-line profiles for shocks of Mach 1.2 for the modified model with a shallower chromospheric temperature increase.

between shock passages; the material is kicked upwards by each shock and then falls back ballistically. The mechanical heating due to the dissipation by preceding shocks is taken into account schematically by raising the model temperature with an amount derived from averaging over many shocks.

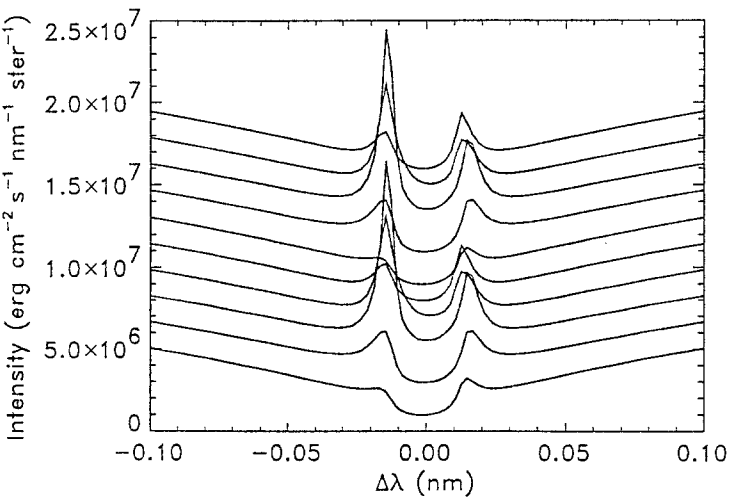

Fig. 13. K-line profiles for shocks of Mach 1.4 for the modified model.

Figures 11, 12, and 13 show three series of resulting profiles. The first is for shock strength Mach 1.2 and model A' while the other series are for shocks with strengths Mach 1.2 and 1.4, respectively, and the modification of model A' shown in Figure 3. The effect of increasing shock amplitude is seen by comparing Figures 12 and 13. It enhances both the violet and the red emission peaks due to the extra mechanical heating.

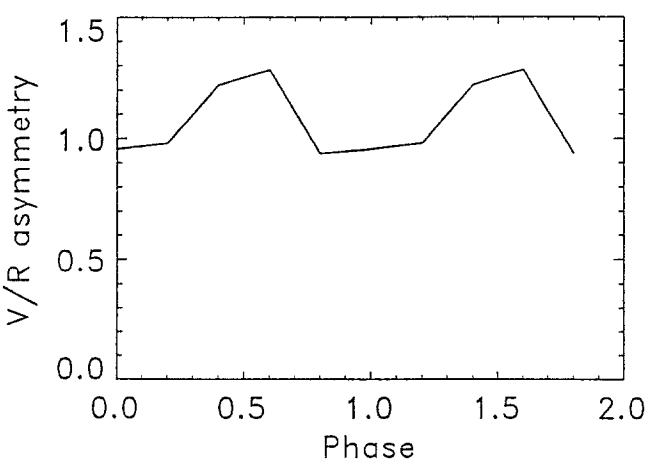

Fig. 14. Ratio of violet over red peak intensities for profiles of Figure 12.

Comparison of Figures 11 and 12 shows the effect of a less steep chromospheric temperature rise which decreases both the red and the blue emission peaks. The V/R ratio, which is shown in Figure 14 for the profiles of Figure 12 is also reduced by this model change. The asymmetric behavior of the K_3 line shift due to the sawtooth velocity field is shown in Figure 15.

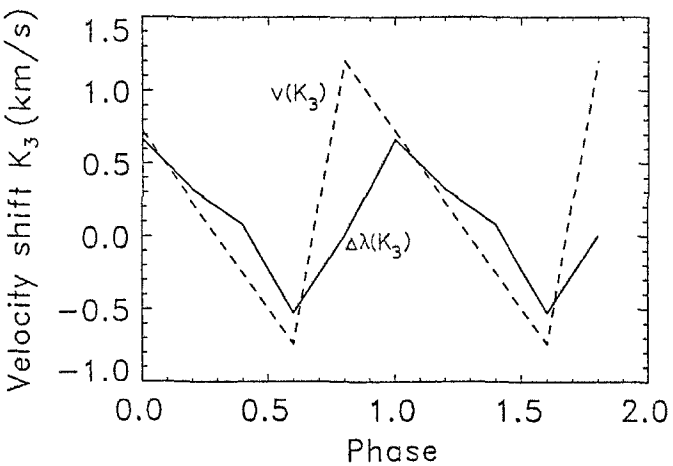

Fig. 15. Velocity shift of K_3 for shocks of Mach 1.2 for the modified model. Coding as in Figure 6.

These computations reproduce observed K_{2V} behavior in displaying appropriate peak asymmetries and K_3 Doppler sequences, but they again produce far too strong K_{2R} emission peaks, too much overall K_{2R} emission and too much K_{2V} emission in the darkest profile. (There is no intensity modulation of the wings because nothing happens below 500 km height in these computations.) Better correspondence may be obtainable from shock trains in which the downward velocities exceed the upward velocities (they are equal here to obtain long-term stability) and by further parameter adjustment; for example, the absence of any peaks in the darkest observed profiles may be reproduced by further change of the chromospheric temperature increase. The extreme model of Holweger and Müller (1974) which has no chromosphere at all indeed produces no peaks at all (Uitenbroek, 1990b).

However, the most important deficiency of this computation is the small amplitude of the K_3 Doppler oscillation which cannot be improved by changes to the atmospheric model. It follows from the small post-shock gas velocity which reaches extrema of only $\pm$ 1.5 km s^{-1}, conform the limiting shock strength described by Ulmschneider (1990) which has post-shock velocities of $0.23c_s$ with c_s the sound velocity. Obtaining larger velocity amplitude requires shocks of larger strength, over Mach 2.

4. Discussion

Our review of observations and modeling efforts in the preceding sections demonstrates that the K_{2V} cell grain phenomenon is quite complex – the absence of a generally accepted explanation is therefore not surprising. However, our extraction of observational constraints in Section 2 and our tests of modeling options in Section 3 give us enough ground to speculate on K_{2V} cell grain formation and to distill a number of implications.

What are the K_{2V} cell grains? Various possibilities are currently debated (Kalkofen, 1989; Deubner, 1991; Rutten and Uitenbroek, 1991; Rammacher and Ulmschneider, 1991). The first is the flux tube scenario of Kalkofen (1989) in which K_{2V} grains mark sites of chromospheric heating which takes place exclusively in strong-field flux tubes. It is supported by the spatial correlation between K_{2V} features and low-flux magnetic elements observed by Sivaraman and Livingston (1982) and by the grain location stability noted by Damé (1985a), but we believe that these wide-passband observations refer not to regular K_{2V} cell grains but to rarer and stronger 'magnetic grains' for which the fluxtube paradigm may indeed hold.

Our main conclusion from the observational literature is that the K_{2V} grains are primarily oscillatory phenomena. They have nothing to do with fluxtube collapse, fluxtube heating, fluxtube motion, small-loop reconnection, siphon flows or other processes related to strong magnetic fields. We do not *a priori* reject causal relationships with weaker magnetic field elements or other discrete structures or impulsive processes, but then admit only those wave actuators which provide ubiquity over the surface in cellular patterning with about 8 Mm wavelength. Kalkofen (1989) weaves the observed 3-min repetitivity of the K_{2V} cell grains and the apparent upward propagation of the Ca II wing whiskers into a fabric of evidence that chromospheric heating occurs only in grains and is due to 3-min waves that are running upward in flux tubes, but network and plages, which do contain strong-field flux tubes, do not share in the 3-min repetitivity and do not show contracting whiskers; these are associated only with cell interiors in which strong-field flux tubes are scarce.

Thus, we submit that the K_{2V} cell grains are of a hydrodynamical nature. The issues of interest are the identification of the pertinent wave modes, the presence or absence of piston excitation and the consequences for the chromospheric energy balance. There are three hydrodynamical scenarios currently under discussion. We briefly present them first and then review pros and cons below.

The first one is the nonlinear wave picture drawn recently by Deubner (1991) at the Heidelberg Conference. He proposes that both the inner-wing whisker brightness modulation and the K_3 Doppler sawtooth oscillation result from 180 s oscillation of the K_3-forming layer which is nonlinear but still subsonic. It is a propagating wave of which the phase lags behind the oscillations which affect the K_{2V}-forming layer. The latter are the oscillations seen in the Ca II 854.2 nm line and comparable lines, with 90° retardation between redshift and brightness. The observed sinusoidal character of this oscillation is Deubner's inspiration to suggest subsonic oscillation rather than shock

behavior for K_3. The scheme is analogous to the wave model of Cram, Brown, and Beckers (1977) but with some nonlinear sawtooth character permitted to K_3.

The second scenario is the one presented by us at the Heidelberg Conference (Rutten and Uitenbroek, 1991) in which the K_{2V} grains display shock heating which takes place when back-falling matter from the previous cycle hits the next updraft in shock trains with 2–3 min periodicity. This scheme mimics the behavior seen in Figure 13 of Leibacher, Gouttebrozes, and Stein (1982), but takes place appreciably lower in the atmosphere. It requires a transition from sinusoidal motion to shock motion between the formation heights of 854.2 nm and K_3 which we attribute to the outward drop in γ (ratio of specific heats, cf. Figure 2 of Gouttebroze (1989)); it also requires strong shocks, with about 5 km s^{-1} post-shock material velocity.

The third scenario is Ulmschneider's in which short-period waves (about 30 s) heat the low chromosphere in non-magnetic cell interiors (e.g., Ulmschneider, 1990). Recent unpublished computations by Rammacher and Ulmschneider (1991) show that these quickly steepen into shock trains already low in the atmosphere. The velocity amplitudes grow until they reach a few km s^{-1}, in agreement with the limiting shock strength of Ulmschneider (1990). There is much vertical interference between successive shocks. Their upward kicks and ballistic downfall may add together; a slower modulation of the average velocity develops with about 180 s periodicity and 4–5 km s^{-1} amplitude. This modulation produces K-core behavior which comes close to the observed standard pattern of K_{2V} cell grains.

At present, we cannot decide unequivocally between these three schemes. We therefore choose to discuss the various ingredients of the K_{2V} cell grain phenomenon with these suggestions in mind.

(i) *Outer-wing whisker modulation.* The outer-wing whiskers are best seen as bar-like structures in the time-resolved modulation spectra in Figure 5 of Cram and Damé. We identify them as the spectral representation of the solar p-mode oscillation in the upper photosphere, consisting of 3–5 min waves. These are diagnosed well by Cram's (k, ω) diagrams up to the height at which the Ca II 854.2 nm line is formed; the analyses of Deubner and Fleck apply to these whiskers as well.

The observed inward progression of the whiskers has often been taken as evidence of upward propagation of temperature disturbances, but Deubner (1990) stresses the important point that this behavior agrees with expectation for non-propagating evanescent waves if one takes radiation losses into account. The $V - I$ phase difference for an adiabatic wave in a stratified atmosphere is 180° for an upward propagating wave and 90° for an evanescent wave, respectively. Radiation losses decrease this lag (Noyes and Leighton, 1963; Schmieder, 1977). At lower altitudes the radiation losses are larger, the gas is further from adiabatic and the lags are smaller. Evanescent waves should therefore have $V - I$ lags that, for increasing height, increase from values below 90° to about 90°. This is indeed observed in all lines and in the K-line features that are formed up to the formation height of the Ca II 854.2 nm line. The same applies to the infrared $I - I$ phase differences observed by Lindsey and Roellig (1987) whose invocation of special damping mechanisms is therefore unnecessary (Deubner, 1990), and for the

$V - I$ phase differences observed for CO lines by Ayres and Brault (1990). Thus, all these oscillation diagnostics indicate evanescent wave behavior; our conclusion that they refer to the outer-wing whiskers then implies that the apparent whisker contraction is simply due to evanescent oscillation with upward (spectrally inward) increasing adiabaticity.

The spatial amplitude pattern over the solar surface (H-wing diagram of Cram and Damé) has small scale structure, about 2–3 Mm typical element size, which results from interference between different wave modes; Cram's (k, ω) diagrams indicate that the actual wavelengths range from 3 to 20 Mm.

(ii) *Inner-wing whisker modulation.* Deubner (1991) attributes the triangular dark inner-wing branches in the time-resolved spectra of Cram and Damé to an intensity modulation caused by absorption in the K_3 forming layer which darkens in phase with the Doppler oscillation of K_3 (darkest at maximum blueshift). It extends across the inner wings; Deubner proposes that its vanishing produces the apparent inward progression of bright whiskers.

We believe instead that the inner-wing whiskers belong to deeper layers. They appear in tandem with the outer-wing whiskers; the larger-scale intensity modulation pattern of the H-wing diagram of Cram and Damé is also seen in the line-core diagrams; the dark triangles have their top at line center at rest; the inner-wing Fourier spectra of Cram fit in the pattern set by the lower-formed diagnostics, in contrast to the K_3 intensity power. A cloud in the K_3 layer that develops sufficient opacity to be seen far out in the wings should be optically very thick at line center.

We propose the following identification. Towards line center more and more high-frequency power mixes into the observed signal since it is formed at larger heights, as follows from the migration towards higher frequencies of the power in Cram's (k, ω) diagrams. Cram's $I - I$ inner-wing phase difference diagrams show lags of increasing duration for higher frequencies, up to 90° at 2 min for the $\Delta\lambda = 0.3$ nm and K_{1V} intensity pair. As noted above, the larger contribution by these longer lags translates into the observed inner-wing whisker slowdown. At the first wavelength the oscillation is evanescent, with $V - I \approx 90°$; since the observed $V - V$ differences are small at large height, it follows that for 2-min waves $V - I \approx 180°$ at the larger height, i.e., that upward propagation occurs.

The same increase to 180° is seen in the $V - I$ phase spectrum for Hα of von Uexküll *et al.* (1989) for cell interiors. They remark that seeing effects comparable to the masquerading as short-period waves by granulation may simulate this behavior. When granulation dances around across the slit, it produces highly correlated high-frequency V and I signals (Endler and Deubner, 1983). In this case it would require strong correlation between brightness and updrafts at 8 Mm spatial wavelengths. This is unlikely. The whisker pattern itself is out of phase in $V - I$; our estimate of 180° lag follows from observed 90° $I - I$ phase difference without velocity signal.

We conclude that, with the increasing contribution of higher-frequency waves closer to line center, the overall character of the oscillation changes from evanescent to propagating acoustic wave behavior. The higher the frequency, the larger the $I - I$ phase

lag; near the H and K cores, the larger contribution with high frequencies results in the observed slow-down of the whisker contractions and the conspicuous triangular shape of the dark inner-wing branches in the time-resolved spectra of Cram and Damé.

(iii) K_3 *Doppler oscillation.* We agree with Deubner and Fleck that 'something drastic happens at 800–1200 km height'; it is shown by the striking change between K_3 morphology and what happens deeper down. In the spatio-temporal domain this change manifests itself in the large difference between the V/R diagram of Cram and Damé and all their other space-time diagrams; in the Fourier domain it shows up as the disappearance of intensity power in Cram's (k, ω) spectra.

The K_3 Doppler oscillation differs notably from the p-mode oscillation in deeper layers. The V/R diagram shows much more horizontal phase propagation and horizontal phase coherence than the H-wing intensity diagram and it displays much less confusion between competing wavelengths and periodicities. While the H-wing diagram resembles a granulation time-slice plot, though with coarser and faster modulation, the V/R diagram looks very much like the space-time phase patterns of the five-minute oscillation. Deubner (1991) points out that the morphology of the V/R diagram reminds one of the debates on the five-minute oscillation before its (k, ω)-ridges were identified, in which the observed variations in coherence over the surface were attributed either to local excitation or to many-mode interference (e.g., p. 324 of Thomas, 1967).

Actually, we equate not the V/R Doppler oscillation but the outer-wing whisker modulation with the interference patterns of the p-mode oscillations; the reason why the H-wing diagram appears less like 5-min diagrams and displays more confusion is that it mixes the lower-frequency evanescent waves with higher-frequency propagating waves which gain importance closer to line center, perhaps with additional smaller and slower modulation by the reversed contrast above granules. The larger resemblance of the V/R diagram to 5-min behavior confirms that the K_3 oscillation is a cleaner oscillation and it suggests that its phase coherency patterns are either due to local excitation or to multi-mode interference.

The K_3 Doppler oscillation has rather well-defined periodicity of 2–3 min and wavelengths of about 8 Mm, best seen in the V/R diagram. The sawtooth Doppler behavior of K_3 in the time-resolved spectra and the large excursions (up to 10 km s^{-1}) indicate strong nonlinearity. In our scenario, the nonlinearity is due to shock behavior when successive fronts in a wavetrain interact; we propose that shock heating occurs when back-falling matter at the end of the free-fall phase reaches large downward velocity and hits the next updraft of upward propagating waves of 2–3 min periodicity. Our shock train computation shows that such trains can impart the observed evolutionary characteristics of the standard pattern on the K-line, but indicates that strong shocks are required at low height. The inner-wing whisker modulation indicates that such propagating waves are indeed present, but it is not clear whether they shock strongly enough deeply enough.

Ulmschneider's scenario of similar vertical interference between the fronts of short-period shock trains is attractive because waves of about 30 s periodicity propagate deeper and easier, shock at lower heights and follow in quicker succession. The observed

3-min periodicity then has to come from modulation in the compression of successive fronts which reaches sufficiently large velocity amplitude from constructive interference by many weak shocks. This is indeed the case in Rammacher's current computations. However, there are no supporting observations of 30 s waves in H and K. The scheme requires long wave trains with high coherence which should be observable in the inner wings of H and K, but such measurements are probably difficult in the presence of atmospheric seeing (cf. Endler and Deubner, 1983). We note that measurements of unresolved non-thermal broadening of blends in the wings of H and K leave sufficient amplitude for a sizable contribution by short-period waves (Ayres, 1977a; Gurtovenko, Sheminova, and Rutten, 1985).

In both scenarios the shocks are narrower than the contribution functions of the Ca II infrared lines and may appear only in their outer tails. We speculate that the competition between the upward motion in the fronts and the ballistic downfall between the fronts masquerades as standing-wave behavior in Fourier spectra, causing the small observed $V - V$ phase lags and also the downward-travelling $V - V$ phase in the Ca II 854.2–849.8 nm $V - V$ pair observed by Deubner and Fleck (1990).

(iv) *Piston excitation.* We ascribe the inner-wing whisker modulation to upward propagating waves with higher frequency than the cutoff frequency; at the K_3 level, they may steepen into nonlinear but subsonic waves as in Deubner's scenario, shock in pairs as in our scenario, or consist of ensembles of shocking short-period waves as in Ulmschneider's scenario. How are these waves excited?

One possibility is that they are globally present, part of the p-modes and due to subsurface turbulent convection just as the 5-min oscillation is thought to be. We cannot decide from the observations reviewed in Section 2 whether such global presence or local piston excitation is more likely. The variations of spatio-temporal phase coherence in the V/R diagram may be taken as evidence of piston excitation but, as noted, may also be due to mode interference. Is there (k, ω) ridge structure for these waves? Cram's (k, ω) diagrams would probably not resolve ridges if they exist; the ridges on the South Pole K-line intensity (k, ω) diagram of Jefferies *et al.* (1988) do extend to 150 s periodicity, but the 10 arc sec pixel size recorded wavelengths above 30 Mm only.

There are various piston candidates. The incidental wave trains of the p-mode interference pattern itself may excite shorter-period waves in 'meso-scale' patterns; the upthrust of large granules, the central downflows above large granules when they 'explode', vortices where mesogranular flows converge, etc., are all pistons that also operate on mesoscales and may thus provide the observed 8 Mm wavelengths.

The 300 s piston of Leibacher, Gouttebroze, and Stein (1982) indeed excited 200 s waves; such 'wakes' of oscillations at the acoustic cutoff frequency are a natural result of propagating disturbances and pulses (Lamb, 1908; Schmidt and Zirker, 1963; Kato, 1966; Souffrin, 1966; Meyer and Schmidt, 1967; Stein and Schwartz, 1972). Recent piston-excitation computations for an isothermal atmosphere by Fleck and Schmitz (1991) show the same phenomenon; it is also found in the granulation simulation of Steffen, Krüss, and Holweger (1991). Thus, the presence of 180 s waves above the temperature minimum only requires a kick to the atmosphere below. Outward tempera-

ture increase causes faster propagation, nonlinear character, possibly reflection and standing-wave behavior.

Evidence for granular piston action has been given by Deubner (1974) and Cram, Brown, and Beckers (1977), who observed instances in which a penetrating granule excited a train of violent chromospheric oscillations with periods around the cutoff frequency. A computational example is furnished by Schmidt and Stix (1973) who extend the granular wave excitation study of Stix (1970) with a phase diagram of granule-excited waves that have 200 s periodicity directly above the granule, while off-axis waves have longer periods, up to 400 s. The elastic granulation simulation of Stein and Nordlund (1989) predicts that horizontal flows around expanding granules contain shocks where they become supersonic (p. 288 of Spruit, Nordlund, and Title, 1990). Stix and Wöhl (1974) have searched for granular-excited horizontal sound waves without success, but the spatial correlation between the long-term intensity of the Mg I b_1 line and the mesogranular flow pattern observed by November (1989) indicates a vertical connection which may be due to granular wave excitation.

(v) *Pattern interference.* Cram (1978) points out that wave explanations suffer from the disparity between the small sizes of the K_{2V} grains (1–2 Mm) and the horizontal wavelengths (about 8 Mm) of the dominant chromospheric oscillations. The shock train explanations also predict cell grains with about the size of a wave crest for every wave crest. In contrast, Gillespie's K_{2V} spectroheliogram and the 160 nm rocket images display small bright points on a background with larger dark areas; positives and negatives are far from reversed equality. Another ingredient is required to explain the smallness of the grains and their scarcity on the surface. The same holds for their large irregularity in amplitude and in repetition interval.

We suggest that this extra ingredient is wave pattern interference, based on our finding that K_{2V} grains occur only where and when the H-wing and the V/R diagrams of Cram and Damé are both bright, i.e., if K_3 is at maximum redshift while the wing modulation is near the end of its bright phase. The striking difference in morphology between these two diagrams results in the grain occurrence patterns. The smallness of the grains conforms to the small extent of these overlaps; the wide spacing follows from the 8 Mm wavelengths of the wavy V/R patterns while the occasional grain clustering follows from the narrow columnar structure in the H-wing diagram. The latter may also produce grain fine structure.

We speculate that the spatio-temporal phase pattern changes with height, along with the transition from dominance by 5-min p-modes in the photosphere to dominance by 2–3 min Doppler oscillation in the chromosphere. Such change is probable if local piston excitation produces the K_3 Doppler oscillation but may also be present if the K_3 oscillation consists of p-mode interference patterns. The differences between the phase patterns then causes the observed disparity between the two diagrams. We thus do not require grain localization by means other than interference, but we note that the grain intensities depend on the size of the K_3 Doppler shift and may therefore vary with local piston properties.

What causes this requirement of bright-bright coincidence between the two patterns?

We offer two suggestions. In the nonlinear but subsonic wave scenario it may be change in horizontal interference modulation with altitude. Such pattern change implies that 2–3 min waves get the chance to display the behavior seen in one-dimensional single-wave computations only in a few locations and over smaller areas.

In the shock scenario, phase knowledge is destroyed at the shock fronts; however, the observed coincidence then implies that grains occur when K_3 matter has the longest way to fall, i.e., when the underlying atmosphere is at maximum compression in its *p*-mode oscillation. For 15 km deep troughs in the *p*-mode interference pattern, back-falling K_3 matter may thus reach an additional 3 km s^{-1} downward velocity. This is enough to provide the observed sawtooth excursions connected to K_{2V} grains if the shock trains reach 5 km s^{-1} amplitude in a stationary atmosphere. Fine structure may be added by granular surface modulation.

(vi) CO *clouds*. How do the cool CO clouds fit into these oscillatory scenarios? Ayres, Testerman, and Brault (1986) placed the clouds in quiet areas of the low chromosphere, above the temperature minimum. Numerical modeling indicates that CO-line cooling can be very important at these heights, leading to 'bifurcation' into either hot or cool solutions of energy balancing (Kneer, 1983; Muchmore and Ulmschneider, 1985; Nordlund, 1985; Muchmore, 1986; Steffen and Muchmore, 1988; Anderson, 1989). The CO clouds might therefore take part in the K_{2V} cell grain phenomenon, leading to the suggestion to look for 3-min oscillatory behavior of the CO lines and for systematic redshifts analogous to the large redshifts which K_3 reaches when the lower chromosphere is maximally compressed. CO cooling might even precipitate this downpour.

However, the recent CO oscillation measurements of Ayres and Brault (1990) address this suggestion with negative results. They confirm the earlier results of Noyes and Hall (1972) that the CO lines display normal 5-min oscillation without a higher-frequency tail. In addition, their $V - I$ phase measurements firmly confirm that the line cores are formed at lower altitudes, only a few hundred km high and below the temperature minimum. The clouds do not, therefore, participate at all in K_3 or K_{2V} phenomena, but belong to the outer-wing whisker patterns or even to the granular overshoot regime.

(vii) *Bright points at 160 nm.* Spatially-averaged models indicate that the 160 nm wavelength region is formed at the temperature minimum. In a recent analysis of HRTS data Cook and Ewing (1991) studied the underlying background intensity of their images, not concentrating on the bright points but on the more diffuse larger-scale pattern. It oscillates with 250 s average periodicity, comparable to the intensity of Na I D_2 in Cram's (k, ω) diagrams and in good agreement with formation around the temperature minimum. Cram's (k, ω) diagrams for the K-line wing intensity show that this oscillation corresponds to the outer-wing whisker modulation, indeed with *p*-mode properties.

The 160 nm bright points are also frequently denoted as temperature-minimum features, but they must be formed much higher. Their 180 s periodicity and their morphology indicate that they originate in the same layer where the K_3 Doppler oscillation occurs and the K_{2V} grains are caused. Cook and Ewing (1991) state that 'the bright points appear to simply float in brightness above the general global 250 s oscillations'; in fact, the points literally form at much higher altitude.

(viii) *Average atmosphere.* Avrett (1985) modified the temperature minimum region of the earlier model grid of Vernazza, Avrett, and Loeser (1981) in order to obtain better agreement with the H-line observations of Cram and Damé and so with the H and K modeling by Ayres and Linsky (1976). The modification also brought the predicted infrared continua into agreement with the observations of Degiacomi, Kneubühl, and Huguenin (1985); the new model therefore reproduces an impressive array of diagnostics (cf. Rutten, 1990b).

However, the infrared observations of Boreiko and Clark (1987) and the spectral line diagnostics of Shchukina, Shcherbina, and Rutten (1990) favour a cooler temperature minimum; shifting the CO clouds from above the temperature minimum to below the temperature minimum now presents a major challenge to the photospheric part. The chromospheric part requires adaptation as well. The simulations of Gouttebroze and Leibacher (1980) and our shock train illustration indicate that even model A' fails to explain H and K profiles from the darkest elements in cell interiors.

(ix) *Chromospheric energy balance.* It may well be that K_{2V} grains display 'the' heating of the quiet chromosphere directly. Our conclusion that the grains are a hydrodynamical phenomenon of oscillatory nature agrees with the 'classical' picture of wave heating (e.g., Biermann, 1946; Schwarzschild, 1948; review by Kuperus, 1969) applied to cell interiors. The shock scenarios imply direct energy dissipation; Deubner (1991) suggests that for the wave scenario the ionization damping mechanism (enthalpy change) of Lindsey (1981) provides sufficient energy deposition.

However, we feel that all terms in the energy balance should be known before the grand total is summed up. Detailed explanation of the K_{2V} cell grains with all the attendant phenomena must come first; also, the cool CO cloud puzzle must first be solved.

(x) *Chromospheric jets.* Another issue is whether the quiet-Sun chromospheric jets observed in C I lines are part of the cell grain phenomenon. The 5–10 km s^{-1} downdrafts of K_3 may be part of cycles in which higher layers reach 10–20 km s^{-1} updrafts; theoretical context is perhaps given by the 'rebound shock model' of Hollweg (1982) (see also Sterling and Hollweg, 1984, 1988, 1989). It was designed for solar spicules but may well apply here. The decisive observation will be to link these jets to 160 nm bright cell points by spatio-temporal correlation, admitting the possibility of phase delay between the one and the other.

(xi) *V/R asymmetry in other stars.* Solar identification of the processes which contribute to the *V/R* asymmetry between K_{2V} and K_{2R} in 'Sun-as-a star' spatially-averaged spectra is of obvious interest to diagnostic application of the *V/R* asymmetries observed for the double Ca II H and K and Mg II h and k peaks from other stars (Dupree, 1976; Stencel, 1978; Cram, Krikorian, and Jefferies, 1979; McClintock *et al.*, 1978; Weiler and Oegerle, 1979; Stencel and Mullan, 1980; Zarro and Rodgers, 1983; Crivellari *et al.*, 1987).

On the Sun, plage emission tends to be symmetric. The plage emission profile derived by Oranje (1983) actually displays slightly reversed asymmetry. Oranje uses it in his Figure 7 to extrapolate the observed solar minimum-activity irradiance profile to zero

line-center intensity; the resulting profile and an intermediate profile have $V/R > 1$. From this, Cram (1983) concludes that the V/R asymmetry of the integrated solar profile is not determined by the plage contribution. He suggests that it is due to the preponderance of K_{2V} grains over K_{2R} grains in cell interiors, whereas Skumanich *et al.* (1984) estimate that the contribution of the K_{2V} cell grains to the Sun-as-a-star flux profile is negligible. Stencel (1978) and Stencel and Mullan (1980) take the reversed ($V/R < 1$) asymmetry seen for later stars as indication of mass loss. Altogether, it is not clear yet whether the K_{2V} cell grain oscillation has stellar overtones.

5. Prospects

The major motivation for compiling this review is to provide guidance from the existing literature to future efforts in cell grain studies. Current developments make it likely that significant advances are in reach, both in observation and in interpretation. We discuss these briefly.

5.1. Observations

Solar Ca II observing goes in stages set by detector technology. The traditional use of photographic plates reached its culmination in the Mt. Wilson and Kitt Peak K_{2V} spectroheliograms. The accent then shifted to computer analysis of sequences of spectra from digitized films, with the Sacramento Peak HIRKHAD data as prime example. Now, CCD detection brings in the taking of digital filtergrams and spectrograms, with increasingly high spatial resolution and stability, thanks to image motion correction by active mirrors, local-area autocorrelation tracking, and new telescopes in sites with superior seeing. In addition, multi-wavelength imaging with the SOUP tunable filter (e.g., Title *et al.*, 1990), multi-slit spectrometry with the MSDP spectrometer (e.g., von Uexküll *et al.*, 1989), and rapid slit-stepping with conventional spectrographs provide the capability to advance from the one-dimensional multi-line diagnostics of Cram (1978) and Cram and Damé (1983) to two-dimensional spectrophotometry.

What should be observed?

(i) *Filtergram sequences.* Obvious observing programs for K_{2V} filtergram sequences are posed by the cell grain location selection and memory issues. Are there 'magnetic grains' as we suggest, and do they migrate to cell boundaries as do intranetwork patches of weak magnetic field (cf. Martin, 1990)? Do grains have long location memory as claimed by Damé (1985a)? Do they result from exploding granules, or follow mesogranular divergence centers or around vortices? Are they triggered by the wave trains in the interference patterns of the 5-min oscillation?

These issues require co-spatial and co-temporal imaging in K_{2V}, the continuum and velocity and magnetic lines, using the other bands to construct maps of the horizontal flows, vorticity, vertical velocity and magnetic fields with which the occurrence of K_{2V} grains can be correlated. Concurrent K_{2V} and K_{2R} sequences are of special interest, using the V/R ratio (or $(V - R)/(V + R)$) as a proxy for K_3 Doppler shift. Such programs have been started using SOUP and other LPARL/OSL equipment with the vacuum refractor of the Swedish Solar Observatory on La Palma.

(ii) *Spectrogram sequences.* Spectrometry offers the important advantage that all spectral elements per spatial element along the slit refer to the same object, so that different spectral lines refer to the same seeing-transformed instantaneous realization on the slit of the same solar surface element. Spectrometry therefore gives reliable phase information for velocity and intensity fluctuations; multi-line spectrometry samples different formation heights. It is worthwhile in particular to measure the H or K core including a large segment (0.3–0.5 nm) of the line wing and the superimposed blends; we recommend the strong Fe I line at 396.93 nm. Issues are the presence of shocks and of short-period waves, wave propagation and wave reflection, piston action, (k, ω) ridges, etc.

The obvious requirements here are to obtain long-duration sequences at high spatial resolution and to proceed from one-dimensional to two-dimensional data gathering, improving on the analyses of Cram (1978) and Cram and Damé (1983). The display formats should follow their examples: $V - V$, $V - I$, and $I - I$ (k, ω) diagrams for power, coherency and phase difference between various features and spatio-temporal evolution movies of various sorts. The first group gives phase information of frequency components, the second group supplies event histories and non-sinusoidal patterns. Network-cell interior distinction should be made throughout.

5.2. Simulations

Our conclusion that K_{2V} grains are of a hydrodynamic nature is a fortunate circumstance since chromospheric radiation hydrodynamics is now amenable to computer simulations with a large degree of realism, which is not the case yet for problems in magneto-hydrodynamics (cf. Durrant, 1990; Zhughzda, 1990). The issues to be addressed first are the nature of the K_3 oscillations and whether or not photospheric pistons are at work; eventually, numerical simulations should reproduce the complete K_{2V} grain phenomenon in detail.

Our results above suggest that one-dimensional simulations may fruitfully follow the examples of Leibacher, Gouttebroze, and Stein (1982) and Gouttebroze (1989) for 2–3 min waves and of Rammacher and Ulmschneider (1991) for short-period waves. It will be important to admit partial redistribution effects in the H and K resonance scattering, to compute radiative cooling and heating in detail, to provide lower boundary conditions with the updrafts and downdrafts of the p-mode interference patterns and of the solar granulation, and to experiment with the overall structure of the spatially-averaged atmosphere. They should have sufficient duration that vertical interference can develop and be sampled in behavior. The display formats should follow the observers' example: detailed Ca II profile sequences, not only for K but also for a few inner- and outer-wing wavelengths as well as the Ca II 854.2 nm and Ca II 849.8 nm lines; Fourier spectra for power, coherency and phase of $V - I$, $V - V$, and $I - I$ between various features.

Multi-dimensional simulations are required eventually. Most analyses so far assume vertical wave propagation but obliquity may be an important aspect; three-dimensional modeling will be required to reproduce the observed surface patterns of the grains.

6. Conclusion

The extensive literature on the K_{2V} grains and related cell-interior phenomena leads us to the conclusion that bright cell grains are of hydrodynamical origin, due to oscillations that are present all over the solar surface but which produce grains only at places and moments set by pattern interference between the velocity oscillations in the K_3 layer and the evanescent wave trains of the *p*-mode oscillation deeper down. They remind us of what is called 'clapotis' on sea charts for areas where wave interference produces waterspouts on the ocean (e.g., Dowd, 1981).

The nature of the K_3 Doppler oscillation remains unresolved. The contenders are (a) subsonic but nonlinear waves of about 3-min periodicity as proposed by Deubner, (b) 2–3 min shock trains with ballistic downfall as proposed by us, and (c) short-period shock sequences with about 3-min modulation in train compression being investigated by Rammacher and Ulmschneider. Piston excitation and pattern memories are not excluded.

Our review leaves us with renewed appreciation of the overwhelming richness which the solar atmosphere offers to terrestrial astrophysicists in order to teach them the physics of astrophysical plasmas (cf. Rutten, 1990a), which indeed requires the holistic approach advocated by Cram in the quotation at the head of this review. We confirm his view by finding that all observations, with whatever diagnostic, of all cell-interior phenomena are relevant to the topic of K_{2V} cell grains. We surmise the reverse holds as well.

We think the K_{2V} grains important, even apart from the obvious interest they provide to the topic of chromospheric energy balancing, because they may well become the first dynamical phenomenon of the solar chromosphere to be understood in detail – a step up from the *p*-modes and the granulation deeper down. We expect that the combination of new observational techniques and advances in numerical simulation will soon answer the question *why* cell grains appear as they do. We are also confident that the cell grains furnish diagnostics of considerable value because their formation is so intricate: the fact that they have never been explained although they are so specific in signature implies that they should be quite informative. We so hope that eventually the cell grains will join the list of valuable Ca II H and K diagnostics and become useful as chromospheric measuring instruments, for the Sun and for other stars.

Acknowledgements

We are indebted to T. R. Ayres, P. N. Brandt, A. A. van Ballegooijen, M. Carlsson, L. E. Cram, F.-L. Deubner, C. J. Durrant, B. Fleck, V. Gaizauskas, W. Kalkofen, M. Martić, D. A. Muchmore, L. J. November, Å. Nordlund, N. R. Sheeley, R. A. Shine, G. W. Simon, H. C. Spruit, R. F. Stein, J.-O. Stenflo, P. Ulmschneider, N. O. Weiss, and C. Zwaan for stimulating oral and email discussions, to L. Damé and G. Artzner for sending unpublished material, to P. N. Brandt, B. W. Lites, and P. Ulmschneider for showing us yet unpublished new results, to A. A. van Ballegooijen

for the use of his shock wave code and assistance in using it, and to L. E. Cram and C. Zwaan for constructive comments on an earlier manuscript (Uitenbroek, 1990a). H. Uitenbroek acknowledges partial support from NASA Grant NSG-7054.

References

Anderson, L. S.: 1989, *Astrophys. J.* **339**, 558.
Artzner, G., Leibacher, J., Vial, J.-C., Lemaire, P., and Gouttebroze, P.: 1978, *Astrophys. J.* **224**, L83.
Athay, R. G.: 1970, *Solar Phys.* **11**, 347.
Athay, R. G. and Dere, K. P.: 1990, *Astrophys. J.* **358**, 710.
Auer, L. H., Rees, D. E., and Stenflo, J. O.: 1980, *Astron. Astrophys.* **88**, 302.
Avrett, E. H.: 1985, in B. W. Lites (ed.), *Chromospheric Diagnostics and Modeling*, National Solar Observatory Summer Conference, Sacramento Peak Observatory, Sunspot, p. 67.
Ayres, T. R.: 1975, *Astrophys. J.* **201**, 799.
Ayres, T. R.: 1977a, *Astrophys. J.* **214**, 905.
Ayres, T. R.: 1977b, *Astrophys. J.* **213**, 296.
Ayres, T. R.: 1981, *Astrophys. J.* **244**, 1064.
Ayres, T. R.: 1990a, in G. Wallerstein (ed.), *Cool Stars, Stellar Systems and the Sun*, Proc. Sixth Cambridge Workshop, Astron. Soc. Pacific Conference Series, Vol. 9, p. 106.
Ayres, T. R.: 1990b, in J.-O. Stenflo (ed.), 'The Solar Photosphere: Structure, Convection and Magnetic Fields', *Proc. IAU Symp.* **138**, 23.
Ayres, T. R. and Brault, J. W.: 1990, *Astrophys. J.* **363**, 705.
Ayres, T. R. and Linsky, J. L.: 1976, *Astrophys. J.* **205**, 874.
Ayres, T. R. and Wiedemann, G. R.: 1989, *Astrophys. J.* **338**, 1033.
Ayres, T. R., Testerman, L., and Brault, J. W.: 1986, *Astrophys. J.* **304**, 542.
Babcock, H. W. and Babcock, H. D.: 1955, *Astrophys. J.* **121**, 349.
Bappu, M. K. V. and Sivaraman, K. R.: 1971, *Solar Phys.* **17**, 316.
Beckers, J. M.: 1964, 'A Study of the Fine Structures in the Solar Chromosphere', Ph.D. Thesis Utrecht University, AFCRL Environmental Research Paper No. 49.
Beckers, J. M. and Artzner, G.: 1974, *Solar Phys.* **37**, 309.
Beckers, J. M. and Milkey, R. W.: 1975, *Solar Phys.* **43**, 289.
Beckers, J. M., Mauter, H. A., Mann, G. R., and Brown, D. R.: 1972, *Solar Phys.* **25**, 81.
Bhatnagar, A. and Tanaka, K.: 1972, *Solar Phys.* **24**, 87.
Biermann, L.: 1946, *Naturwissenschaften* **33**, 118.
Bonnet, R. M., Lemaire, P., Vial, J.-C., Artzner, G., Gouttebroze, P., Jouchoux, A., Leibacher, J. W., Skumanich, A., and Vidal-Madjar, A.: 1978, *Astrophys. J.* **221**, 1032.
Bonnet, R. M., Bruner, E. C., Acton, L. W., Brown, W. A., and Decaudin, M.: 1980, *Astrophys. J.* **237**, L47.
Bonnet, R. M., Bruner, M., Acton, L. W., Brown, W. A., Decaudin, M., and Foing, B.: 1982, *Astron. Astrophys.* **111**, 125.
Boreiko, R. T. and Clark, T. A.: 1987, *Astrophys. J.* **318**, 445.
Brandt, P. N., Ferguson, S., Scharmer, G. B., Shine, R. A., Tarbell, T. D., Title, A. M., and Topka, K.: 1989, in O. von der Lühe (ed.), *High Spatial Resolution Solar Observations*, 10th Sacramento Peak Summer Workshop, NSO, Sunspot, New Mexico, p. 473.
Brueckner, G. E.: 1980, *Highlights of Astronomy (IAU)* **5**, 557.
Caccin, B., Gomez, M.-T., Marmolino, C., and Severino, G.: 1977, *Astron. Astrophys.* **54**, 227.
Canfield, R. C.: 1971, *Astron. Astrophys.* **10**, 64.
Canfield, R. C.: 1976, *Solar Phys.* **50**, 239.
Canfield, R. C. and Beckers, J. M.: 1976, in R. Cayrel and M. Steinberg (eds.), *Physique des mouvements dans les atmosphères stellaires*, Colloques Internationaux No. 250, CNRS, Paris, p. 273.
Canfield, R. C. and Musman, S.: 1973, *Astrophys. J.* **184**, L131.
Cook, J. W. and Ewing, J. A.: 1991, *Astrophys. J.* (in press).
Cook, J. W., Brueckner, G. E., and Bartoe, J.-D. F.: 1983, *Astrophys. J.* **270**, L89.
Cram, L. E.: 1972a, *Solar Phys.* **22**, 375.
Cram, L. E.: 1972b, *Proc. Astr. Soc. Australia* **2**, 146.

Cram, L. E.: 1974, *Solar Phys.* **37**, 75.
Cram, L. E.: 1976, *Astron. Astrophys.* **50**, 263.
Cram, L. E.: 1978, *Astron. Astrophys.* **70**, 345.
Cram, L. E.: 1983, *Proc. Astron. Soc. Australia* **5**, 152.
Cram, L. E. and Damé, L.: 1983, *Astrophys. J.* **272**, 355.
Cram, L. E., Brown, D. R., and Beckers, J. M.: 1977, *Astron. Astrophys.* **57**, 211.
Cram, L. E., Krikorian, R., and Jefferies, J. T.: 1979, *Astron. Astrophys.* **71**, 14.
Cram, L. E., Rutten, R. J., and Lites, B. W.: 1980, *Astrophys. J.* **241**, 374.
Crivellari, L., Beckman, J. E., Foing, B. H., and Vladilo, G.: 1987, *Astron. Astrophys.* **174**, 127.
Damé, L.: 1984, in S. L. Keil (ed.), *Small-Scale Dynamical Processes in Quiet Stellar Atmospheres*, National Solar Observatory Summer Conference, Sacramento Peak Observatory, Sunspot, New Mexico, p. 54.
Damé, L.: 1985a, in H. U. Schmidt (ed.), *Theoretical Problems in High Resolution Solar Physics*, MPA/LPARL Workshop, Max-Planck-Institut für Physik und Astrophysik MPA 212, München, p. 241.
Damé, L.: 1985b, in H. U. Schmidt (ed.), *Theoretical Problems in High Resolution Solar Physics*, MPA/LPARL Workshop, Max-Planck-Institut für Physik und Astrophysik MPA 212, München, p. 244.
Damé, L. and Martić, M.: 1987, *Astrophys. J.* **314**, L15.
Damé, L. and Martić, M.: 1988, in J. Christensen-Dalsgaard and S. Frandsen (eds.), 'Advances in Helio- and Asteroseismology', *IAU Symp.* **123**, 433.
Damé, L., Gouttebroze, P., and Malherbe, J.-M.: 1984, *Astron. Astrophys.* **130**, 331.
Damé, L., Foing, B., Martić, M., Bruner, M. E., Brown, W. A., Decaudin, M., and Bonnet, R. M.: 1986, *Adv. Spac. Res.* **6**, 273.
Degiacomi, C. G., Kneubühl, F. K., and Huguenin, D.: 1985, *Astrophys. J.* **298**, 918.
De Jager, C.: 1959, in S. Flügge (ed.), 'Astrophysik III: Das Sonnensystem', *Handbuch der Physik*, Band 52, Springer-Verlag, Berlin, p. 80.
Deming, D., Glenar, D. A., Käufl, H. U., Hill, A. A., and Espenak, F.: 1986, *Nature* **322**, 232.
Deming, D., Boyle, R. J., Jennings, D. E., and Wiedemann, G.: 1988, *Astrophys. J.* **333**, 978.
Dere, K. P., Bartoe, J.-D. F., and Brueckner, G. E.: 1983, *Astrophys. J.* **267**, L65.
Dere, K. P., Bartoe, J.-D. F., and Brueckner, G. E.: 1986, *Astrophys. J.* **305**, 947.
Desikachary, K. and Gray, D. F.: 1978, *Astrophys. J.* **226**, 907.
Deslandres, H.: 1892, *Compt. Rend. Acad. Sci. France* **114**, 276.
Deslandres, H.: 1910, *Ann. Obs. Paris Meudon* **4**, part 1.
Deubner, F.-L.: 1974, in R. G. Athay (ed.), 'Chromospheric Fine Structure', *IAU Symp.* **56**, 263.
Deubner, F.-L.: 1989a, in R. J. Rutten and G. Severino (eds.), *Solar and Stellar Granulation*, NATO ASI Series C-263, Kluwer Academic Publishers, Dordrecht, p. 195.
Deubner, F.-L.: 1989b, *Astron. Astrophys.* **216**, 259.
Deubner, F.-L.: 1990, in J.O. Stenflo (ed.), 'The Solar Photosphere: Structure, Convection and Magnetic Fields', *Proc. IAU Symp.* **138**, 217.
Deubner, F.-L.: 1991, in P. Ulmschneider, E. Priest, and B. Rosner (eds.), *Mechanisms of Chromospheric and Coronal Heating*, Heidelberg Conference, Springer-Verlag, Berlin (in press).
Deubner, F.-L. and Fleck, B.: 1989, *Astron. Astrophys.* **213**, 423.
Deubner, F.-L. and Fleck, B.: 1990, *Astron. Astrophys.* **228**, 506.
Deubner, F.-L., Fleck, B., Marmolino, C., and Severino, G.: 1990, *Astron. Astrophys.* **236**, 509.
Dowd, J.: 1981, *Sea Kayaking*, University of Washington Press, Seattle.
Dupree, A. K.: 1976, in R. Cayrel and M. Steinberg (eds.), *Physique des mouvements dans les atmosphères stellaires*, Colloq. No. 250, CNRS, Paris, p. 439.
Durrant, C. J.: 1990, in J.-O. Stenflo (ed.), 'The Solar Photosphere: Structure, Convection and Magnetic Fields', *Proc. IAU Symp.* **138**, 489.
Durrant, C. J., Grossmann-Doerth, U., and Kneer, F. J.: 1976, *Astron. Astrophys.* **51**, 95.
Duvall, T., Livingston, W. C., and Mahaffey, C.: 1980, in H. A. Hill and W. A. Dziembowski (eds.), *Nonradial and Nonlinear Stellar Pulsation*, Springer-Verlag, New York, p. 237.
Duvall, T. L., Harvey, J. W., Libbrecht, K. G., Popp, B. D., and Pomerantz, M. A.: 1988, *Astrophys. J.* **324**, 1158.
Endler, F. and Deubner, F.-L.: 1983, *Astron. Astrophys.* **121**, 291.
Engvold, O. and Marstad, N. C.: 1983, *Solar Center-Limb Variation of the Ca II K Line and the Wilson–Bappu Effect*, Reports of the Institute of Theoretical Astronomy No. 55, University of Oslo.
Evans, J. W. and Catalano, C. P.: 1972, *Solar Phys.* **27**, 299.

Evans, J. W., Michard, R., and Servajean, R.: 1963, *Ann. Astrophys.* **26**, 368.
Fleck, B. and Deubner, F.-L.: 1989, *Astron. Astrophys.* **224**, 245.
Fleck, B. and Schmitz, F.: 1991, in P. Ulmschneider, E. Priest, and B. Rosner (eds.), *Mechanisms of Chromospheric and Coronal Heating*, Heidelberg Conference, Springer-Verlag, Berlin, p. 22.
Foing, B. and Bonnet, R. M.: 1984a, *Astron. Astrophys.* **136**, 133.
Foing, B. and Bonnet, R. M.: 1984b, *Astrophys. J.* **279**, 848.
Foing, B., Bonnet, R.-M., and Bruner, M.: 1986, *Astron. Astrophys.* **162**, 292.
Frazier, E. N.: 1968, *Astrophys. J.* **152**, 557.
Fredga, K.: 1971, *Solar Phys.* **21**, 60.
Gaizauskas, V.: 1985, in B. W. Lites (ed.), *Chromospheric Diagnostics and Modeling*, National Solar Observatory Summer Conference, Sacramento Peak Observatory, Sunspot, New Mexico, p. 25.
Giovanelli, R.: 1975, *Solar Phys.* **44**, 299.
Giovanelli, R. G.: 1974, *Solar Phys.* **37**, 301.
Gouttebroze, P.: 1989, *Astrophys. J.* **337**, 536.
Gouttebroze, P., Damé, L., and Malherbe, J.-M.: 1984, *Mem. Soc. Astron. Ital.* **55**, 245.
Gouttebroze, P. and Leibacher, J. W.: 1980, *Astrophys. J.* **238**, 1134.
Grossmann-Doerth, U., Kneer, F., and von Uexküll, M.: 1974, *Solar Phys.* **37**, 85.
Gurtovenko, E. A., Sheminova, V. A., and Rutten, R. J.: 1985, *Soviet Astron.* **29**, 72.
Hale, G. E.: 1892, *Astron. Astrophys.* **11**, 159.
Hale, G. E. and Ellerman, F.: 1904, *Astrophys. J.* **19**, 41.
Hammer, R. and Ulmschneider, P.: 1978, *Astron. Astrophys.* **65**, 273.
Heasley, J. N.: 1975, *Solar Phys.* **44**, 275.
Hollweg, J. V.: 1982, *Astrophys. J.* **257**, 345.
Holweger, H. and Kneer, F.: 1989, in R. J. Rutten and G. Severino (eds.), *Solar and Stellar Granulation*, NATO ASI Series C-263, Kluwer Academic Publishers, Dordrecht, Holland, p. 173.
Holweger, H. and Müller, E. A.: 1974, *Solar Phys.* **39**, 19.
Howard, R.: 1959, *Astrophys. J.* **130**, 193.
Howard, R.: 1962, *Astrophys. J.* **136**, 211.
Hummer, D. and Rybicki, G.: 1968, *Astrophys. J.* **153**, L107.
Jefferies, J. T. and Thomas, R. N.: 1960, *Astrophys. J.* **131**, 695.
Jefferies, S. M., Pomerantz, M. A., Duvall, T. L., Harvey, J. W., and Jaksha, D. B.: 1988, in E. Rolfe (ed.), *Seismology of the Sun and Sun-like Stars*, Proc. ESA-IAC Symposium, ESA SP-286, p. 279.
Jensen, E. and Orrall, F. Q.: 1963, *Astrophys. J.* **138**, 252.
Jewell, L. E.: 1900, *Astrophys. J.* **11**, 234.
Kalkofen, W.: 1989, *Astrophys. J.* **346**, L37.
Kalkofen, W. and Ulmschneider, P.: 1977, *Astron. Astrophys.* **57**, 193.
Kato, S.: 1966, *Astrophys. J.* **144**, 326.
Kelch, W. L. and Linsky, J. L.: 1978, *Solar Phys.* **58**, 37.
Kelch, W. L., Linsky, J. L., and Worden, S. P.: 1979, *Astrophys. J.* **229**, 700.
Kneer, F.: 1983, *Astron. Astrophys.* **128**, 311.
Kneer, F. and von Uexküll, M.: 1983, *Astron. Astrophys.* **119**, 124.
Kneer, F. and von Uexküll, M.: 1985, *Astron. Astrophys.* **144**, 443.
Kneer, F. and von Uexküll, M.: 1986, *Astron. Astrophys.* **155**, 178.
Kneer, F., Newkirk, G., and von Uexküll, M.: 1982, *Astron. Astrophys.* **113**, 129.
Kuperus, M.: 1969, *Space Sci. Rev.* **9**, 713.
Lamb, H.: 1908, *Proc. London Math. Soc.* **7**, 122.
Leibacher, J., Gouttebroze, P., and Stein, R. F.: 1982, *Astrophys. J.* **258**, 393.
Leifsen, T. and Maltby, P.: 1990, *Solar Phys.* **125**, 241.
Leighton, R. B.: 1959, *Astrophys. J.* **130**, 366.
Leighton, R. B.: 1961, in R. N. Thomas (ed.), 'Aerodynamic Phenomena in Stellar Atmospheres', *IAU Symp.* **12**, 430.
Lemaire, P., Gouttebroze, P., Vial, J.-C., and Artzner, G. E.: 1981, *Astron. Astrophys.* **103**, 160.
Lindsey, C. and Roellig, T.: 1987, *Astrophys. J.* **313**, 877.
Lindsey, C. A.: 1981, *Astrophys. J.* **244**, 659.
Linsky, J. L.: 1980, *Ann. Rev. Astron. Astrophys.* **18**, 439.
Linsky, J. L. and Avrett, E. H.: 1970, *Publ. Astron. Soc. Pacific* **82**, 169.

Lites, B. W. (ed.): 1985a, *Chromospheric Diagnostics and Modeling*, Proceedings NSO Summer Conference, Sacramento Peak Observatory, Sunspot, New Mexico.
Lites, B. W.: 1985b, in H. U. Schmidt (ed.), *Theoretical Problems in High Resolution Solar Physics*, MPA/LPARL Workshop, Max-Planck-Institut für Physik und Astrophysik MPA 212, München, p. 273.
Lites, B. W. and Chipman, E. G.: 1979, *Astrophys. J.* **213**, 570.
Lites, B. W., Chipman, E. G., and White, O. R.: 1982, *Astrophys. J.* **253**, 367.
Liu, S.-Y.: 1974, *Astrophys. J.* **189**, 359.
Liu, S. Y. and Sheeley, N. R.: 1971, *Solar Phys.* **20**, 282.
Liu, S.-Y. and Skumanich, A.: 1974, *Solar Phys.* **38**, 105.
Liu, S.-Y. and v. P. Smith, E.: 1972, *Solar Phys.* **24**, 301.
Liu, S. Y., Sheeley, N. R., and v. P. Smith, E.: 1972, *Solar Phys.* **23**, 289.
Livingston, W. C., Harvey, J., Slaughter, C., and Trumbo, D.: 1976, *Appl. Optics* **15**, Part 1, 40.
Machado, M. E., Emslie, A. G., and Brown, J. C.: 1978, *Solar Phys.* **58**, 363.
Magain, P.: 1986, *Astron. Astrophys.* **163**, 135.
Marmolino, C. and Severino, G.: 1990, in J.-O. Stenflo (ed.), 'The Solar Photosphere: Structure, Convection and Magnetic Fields', *Proc. IAU Symp.* **138**, 251.
Martić, M. and Damé, L.: 1989, in R. J. Rutten and G. Severino (eds.), *Solar and Stellar Granulation*, NATO ASI Series C-263, Kluwer Academic Publishers, Dordrecht, Holland, p. 207.
Martin, S. F.: 1990, in J.-O. Stenflo (ed.), 'The Solar Photosphere: Structure, Convection and Magnetic Fields', *Proc. IAU Symp.* **138**, 129.
Mattig, W. and Kneer, F.: 1981, *Astron. Astrophys.* **93**, 20.
McClintock, W., Moos, H. W., Henry, R. C., Linsky, J. L., and Barker, E. S.: 1978, *Astrophys. J.* **202**, 733.
Mein, N.: 1978, *Solar Phys.* **59**, 3.
Mein, P.: 1964, *Compt. Rend.* **258**, 819.
Mein, P.: 1966, *Ann. Astrophys.* **29**, 153.
Mein, P.: 1971, *Solar Phys.* **20**, 3.
Mein, N. and Mein, P.: 1976, *Solar Phys.* **49**, 231.
Mein, N. and Mein, P.: 1980, *Astron. Astrophys.* **84**, 96.
Mein, P., Mein, N., Malherbe, J. M., and Damé, L.: 1987, *Astron. Astrophys.* **177**, 283.
Meyer, F. and Schmidt, H.-U.: 1967, *Z. Astrophys.* **65**, 274.
Middelkoop, F.: 1982, 'Ca II H and K Emission from Late-Type Stars', Ph.D. Thesis, Utrecht University.
Mihalas, D. and Kunasz, P. B.: 1986, *J. Compt. Phys.* **64**, 1.
Mihalas, D. and Mihalas, B. W.: 1984, *Foundations of Radiation Hydrodynamics*, Oxford University Press, New York.
Milkey, R. W., Shine, R. A., and Mihalas, D.: 1975a, *Astrophys. J.* **202**, 250.
Milkey, R. W., Shine, R. A., and Mihalas, D.: 1975b, *Astrophys. J.* **199**, 718.
Miyamoto, S.: 1958, *Publ. Astron. Soc. Japan* **9**, 146.
Muchmore, D.: 1986, *Astron. Astrophys.* **155**, 172.
Muchmore, D. and Ulmschneider, P.: 1985, *Astron. Astrophys.* **142**, 393.
Nordlund, Å.: 1985, in H. U. Schmidt (ed.), *Theoretical Problems in High Resolution Solar Physics*, MPA/LPARL Workshop, Max-Planck-Institut für Physik und Astrophysik MPA 212, München, p. 1.
November, L. J.: 1989, *Astrophys. J.* **344**, 494.
November, L. J., Toomre, J., Gebbie, K. B., and Simon, G. W.: 1981, *Astrophys. J.* **245**, L123.
Noyes, R. W.: 1967, in R. N. Thomas (ed.), 'Aerodynamic Phenomena in Stellar Atmospheres', *IAU Symp.* **28**, 293.
Noyes, R. W. and Hall, D. N. B.: 1972, *Astrophys. J.* **176**, L89.
Noyes, R. W. and Leighton, R. B.: 1963, *Astrophys. J.* **138**, 631.
Noyes, R. W., Baliunas, S. L., Belserene, E., Duncan, D. K., Horne, J., and Widrow, L.: 1984, *Astrophys. J.* **285**, L23.
Oda, N.: 1984, *Solar Phys.* **93**, 243.
Oranje, B. J.: 1983, *Astron. Astrophys.* **124**, 43.
Oranje, B. J.: 1985, 'Solar-type Stellar Chromospheres', Ph.D. Thesis, Utrecht University.
Orrall, F. Q.: 1965, *Astrophys. J.* **141**, 1131.
Orrall, F. Q.: 1966, *Astrophys. J.* **143**, 917.
Owocki, S. P. and Auer, L. H.: 1980, *Astrophys. J.* **241**, 448.
Pasachoff, J. M.: 1970, *Solar Phys.* **12**, 202.

Provost, J. and Mein, N.: 1979, *Solar Phys.* **64**, 43.
Punetha, L. M.: 1974, *Bull. Astron. Inst. Czech.* **25**, 212.
Rammacher, W. and Ulmschneider, P.: 1991, in preparation.
Rottman, G. J., Hassler, D. M., Jones, M. D., and Orrall, F. Q.: 1990, *Astrophys. J.* **358**, 693.
Rutten, R. G. M.: 1987, 'Magnetic Activity of Cool Stars and Its Dependence on Rotation and Evolution', Ph.D. Thesis, Utrecht University.
Rutten, R. J.: 1990a, in J.-O. Stenflo (ed.), 'Solar Photosphere: Structure, Convection and Magnetic Fields', *IAU Symp.* **138**, 501.
Rutten, R. J.: 1990b, in G. Wallerstein (ed.), *Cool Stars, Stellar Systems and the Sun*, Proc. Sixth Cambridge Workshop, Astron. Soc. Pac. Conference Series, Vol. 9, p. 91.
Rutten, R. J. and Severino, G. (eds.): 1989, *Solar and Stellar Granulation*, NATO ASI Series C-263, Kluwer Academic Publishers, Dordrecht, Holland.
Rutten, R. J. and Stencel, R. E.: 1980, *Astron. Astrophys. Suppl. Ser.* **39**, 415.
Rutten, R. J. and Uitenbroek, H.: 1991, in P. Ulmschneider, E. Priest, and B. Rosner (eds.), *Mechanisms of Chromospheric and Coronal Heating*, Heidelberg Conference, Springer-Verlag, Berlin (in press).
Samain, D.: 1991, *Astron. Astrophys.* (in press).
Scharmer, G. B.: 1984, in W. Kalkofen (ed.), *Methods in Radiative Transfer*, Cambridge University Press, Cambridge, p. 173.
Scharmer, G. B. and Carlsson, M.: 1985, *J. Comp. Phys.* **59**, 56.
Schmidt, H. U. and Stix, M.: 1973, *Mitt. Astron. Ges.* **32**, 182.
Schmidt, H. U. and Zirker, J. B.: 1963, *Astrophys. J.* **138**, 1310.
Schmieder, B.: 1976, *Solar Phys.* **47**, 435.
Schmieder, B.: 1977, *Solar Phys.* **54**, 269.
Schmieder, B.: 1978, *Solar Phys.* **57**, 245.
Schoolman, S. A.: 1972, *Solar Phys.* **22**, 344.
Schrijver, C. J.: 1986, 'Stellar Magnetic Activity. Complementing Conclusions Based on Solar and Stellar Observations', Ph.D. Thesis, Utrecht University.
Schrijver, C. J., Dobson, A. K., and Radick, R. R.: 1989, *Astrophys. J.* **341**, 1035.
Schrijver, C. J., Coté, J., Zwaan, C., and Saar, S. H.: 1989, *Astrophys. J.* **337**, 964.
Schwarzschild, M.: 1948, *Astrophys. J.* **107**, 1.
Shchukina, N. G., Shcherbina, T. G., and Rutten, R. J.: 1990, in J.-O. Stenflo (ed.), 'Solar Photosphere: Structure, Convection and Magnetic Fields', *IAU Symp.* **138**, 29.
Shine, R. A. and Linsky, J. L.: 1972, *Solar Phys.* **25**, 357.
Shine, R. A. and Linsky, J. L.: 1974, *Solar Phys.* **39**, 49.
Shine, R. A. and Oster, L.: 1973, *Astron. Astrophys.* **29**, 7.
Shine, R. A., Milkey, R. W., and Mihalas, D.: 1975a, *Astrophys. J.* **199**, 724.
Shine, R. A., Milkey, R. W., and Mihalas, D.: 1975b, *Astrophys. J.* **201**, 222.
Simon, G. W. and Leighton, R. B.: 1964, *Astrophys. J.* **140**, 1120.
Simon, M. and Shimabukuro, F. I.: 1971, *Astrophys. J.* **168**, 525.
Sivaraman, K. R.: 1982, *Astrophys. J.* **254**, 814.
Sivaraman, K. R.: 1991, in P. Ulmschneider, E. Priest, and B. Rosner (eds.), *Mechanisms of Chromospheric and Coronal Heating*, Heidelberg Conference, Springer-Verlag, Berlin (in press).
Sivaraman, K. R. and Livingston, W. C.: 1982, *Solar Phys.* **80**, 227.
Skumanich, A., Smythe, C., and Frazier, E. N.: 1975, *Astrophys. J.* **200**, 747.
Skumanich, A., Lean, J. L., White, O. R., and Livingston, W. C.: 1984, *Astrophys. J.* **282**, 776.
Solanki, S., Steiner, O., and Uitenbroek, H.: 1991, *Astron. Astrophys.* (in press).
Souffrin, P.: 1966, *Ann. Astrophys.* **29**, 55.
Spruit, H. C., Nordlund, Å., and Title, A. M.: 1990, *Ann. Rev. Astron. Astrophys.* **28**, 263.
Steffen, M., Krüss, A., and Holweger, H.: 1991, in P. Ulmschneider, E. Priest, and B. Rosner (eds.), *Mechanisms of Chromospheric and Coronal Heating*, Heidelberg Conference, Springer-Verlag, Berlin (in press).
Steffen, M. and Muchmore, D.: 1988, *Astron. Astrophys.* **193**, 281.
Stein, R. F. and Nordlund, Å.: 1989, *Astrophys. J.* **342**, L95.
Stein, R. F. and Schwartz, R. A.: 1972, *Astrophys. J.* **177**, 807.
Stencel, R. E.: 1978, *Astrophys. J.* **223**, L37.

Stencel, R. E. and Mullan, D. J.: 1980, *Astrophys. J.* **238**, 221.
Stenflo, J. O.: 1980, *Astron. Astrophys.* **84**, 68.
Stenflo, J. O., Baur, T. G., and Elmore, D. F.: 1980, *Astron. Astrophys.* **84**, 60.
Sterling, A. C. and Hollweg, J. V.: 1984, *Astrophys. J.* **285**, 843.
Sterling, A. C. and Hollweg, J. V.: 1988, *Astrophys. J.* **327**, 950.
Sterling, A. C. and Hollweg, J. V.: 1989, *Astrophys. J.* **343**, 985.
Stix, M.: 1970, *Astron. Astrophys.* **4**, 189.
Stix, M. and Wöhl, H.: 1974, *Solar Phys.* **37**, 63.
StJohn, C. E.: 1910, *Astrophys. J.* **32**, 36.
Suemoto, Z.: 1963, *Publ. Astron. Soc. Japan* **15**, 531.
Suemoto, Z., Hiei, E., and Nakagomi, Y.: 1987, *Solar Phys.* **112**, 59.
Suemoto, Z., Hiei, E., and Nakagomi, Y.: 1990, *Solar Phys.* **127**, 11.
Tarbell, T., Ferguson, S., Frank, Z., Shine, R., Title, A., and Topka, K.: 1990, in J.-O. Stenflo (ed.), 'The Solar Photosphere: Structure, Convection and Magnetic Fields', *Proc. IAU Symp.* **138**, 147.
Thomas, R. N. (ed.): 1967, 'Aerodynamic Phenomena in Stellar Atmospheres', *Proc. IAU Symp.* **28**.
Title, A. M.: 1966, *Selected Spectroheliograms*, Mount Wilson and Palomar Observatories, Pasadena.
Title, A. M., Shine, R. A., Tarbell, T. D., Topka, K. P., and Scharmer, G. B.: 1990, in J.-O. Stenflo (ed.), 'The Solar Photosphere: Structure, Convection and Magnetic Fields', *Proc. IAU Symp.* **138**, 49.
Uitenbroek, H.: 1989a, *Astron. Astrophys.* **216**, 310.
Uitenbroek, H.: 1989b, *Astron. Astrophys.* **213**, 360.
Uitenbroek, H.: 1990a, 'Partial Redistribution Modeling of the Ca II K Line', Ph.D. Thesis, Utrecht University.
Uitenbroek, H.: 1990b, in G. Wallerstein (ed.), *Cool Stars, Stellar Systems and the Sun*, Proc. Sixth Cambridge Workshop, Astron. Soc. Pacific Conference Series, Vol. 9, p. 103.
Ulmschneider, P.: 1986, in W. Deinzer, M. Knölker, and H. H. Voigt (eds.), *Small Scale Magnetic Flux Concentrations in the Solar Photosphere*, Abhandl. Akad. Wiss. Göttingen, Math.-Phys. Klasse Dritte Folge No. 38, Vandenhoeck und Ruprecht, Göttingen, p. 191.
Ulmschneider, P.: 1990, in G. Wallerstein (ed.), *Cool Stars, Stellar Systems and the Sun*, Proc. Sixth Cambridge workshop, Astron. Soc. Pacific Conference Series, Vol. 9, p. 3.
Ulmschneider, P., Muchmore, D., and Kalkofen, W.: 1987, *Astron. Astrophys.* **177**, 292.
Ulmschneider, P., Kalkofen, W., Nowak, T., and Bohn, U.: 1977, *Astron. Astrophys.* **54**, 61.
Vardavas, I. M. and Cram, L. E.: 1974, *Solar Phys.* **38**, 367.
Vaughan, A. H., Baliunas, S. L., Baliunas, F. M., Hartmann, L. W., Mihalas, D., Noyes, R. W., and Preston, G. W.: 1981, *Astrophys. J.* **250**, 276.
Vernazza, J. E., Avrett, E. H., and Loeser, R.: 1981, *Astrophys. J. Suppl. Ser.* **45**, 635.
von Uexküll, M., Kneer, F., Malherbe, J. M., and Mein, P.: 1989, *Astron. Astrophys.* **208**, 290.
Walton, S. R.: 1987, *Astrophys. J.* **312**, 909.
Watanabe, T. and Steenbock, W.: 1986, *Astron. Astrophys.* **165**, 163.
Weiler, E. and Oegerle, W.: 1979, *Astrophys. J. Suppl. Ser.* **39**, 537.
White, O. R. and Livingston, W. C.: 1981, *Astrophys. J.* **249**, 798.
Wilson, O. C. and Bappu, M. K. V.: 1957, *Astrophys. J.* **125**, 661.
Wilson, P. R. and Evans, C. D.: 1971, *Solar Phys.* **18**, 29.
Wilson, P. R., Rees, D. E., Beckers, J. M., and Brown, D. R.: 1972, *Solar Phys.* **25**, 86.
Young, C. A.: 1872, *Am. J. Sci.* **104**, 356.
Yudin, O. I.: 1968, *Soviet Phys.-Doklady* **13**, 503.
Zarro, D. M. and Rodgers, A. W.: 1983, *Astrophys. J. Suppl. Ser.* **53**, 815.
Zhughzda, Y. D.: 1990, in L. Deszö (ed.), *The Dynamic Sun*, Proceedings EPS 6th European Solar Meeting, Publ. Debrecen Heliophysical Observatory, Debrecen, Vol. 7, p. 290.
Zirin, H.: 1974, *Solar Phys.* **38**, 91.
Zirin, H.: 1988, *Astrophysics of the Sun*, Cambridge University Press, Cambridge.